INTERFACIAL CHARACTERIZATION OF FIBROUS COMPOSITES BY COHESIVE ZONE METHOD

A Thesis
Submitted to the Graduate Faculty
of the
North Dakota State University
of Agriculture and Applied Science

By
Romit Sarkar

In Partial Fulfillment
for the Degree of
MASTER OF SCIENCE

Major Department:
Mechanical Engineering

August 2012

Fargo, North Dakota

North Dakota State University
Graduate School

Title

Interfacial characterization of fibrous composites by cohesive zone method

By

Romit Sarkar

The Supervisory Committee certifies that this ***disquisition*** complies with North Dakota State University's regulations and meets the accepted standards for the degree of

MASTER OF SCIENCE

SUPERVISORY COMMITTEE:

Dr. Ghodrat Karami
Chair

Dr. Fardad Azarmi

Dr. Mariusz Ziejewski

Dr. Eakalak Khan

Approved:

3/19/2013
Date

Dr. Alan Kallmeyer
Department Chair

ABSTRACT

This work deals with investigation of the interface between unidirectional E-glass fiber and epoxy matrix composites. The two parts in this work are: 1. A periodically constrained finite element (FE) model built as a Representative Volume Element (RVE). 2. A second FE model to predict the shear properties of the interface of the composite.

The first model was built to examine validity of cohesive zone elements of the FE package. Properties of the interface were incorporated into the second model with the help of experimental pull-out test results. A parametric study of the cohesive zone was conducted by variation of its characteristics in the second part.

The load carrying capacity of a composite material is based on its ability to transfer the stress between its components. The results of this study yielded findings about stress patterns of the interface responsible for the load transfer from the fiber to the matrix.

ACKNOWLEDGEMENTS

I would like to thank my advisor, Dr. Ghodrat Karami for the constant support and encouragement that he provided me as I conducted my research. Throughout the period of my master's degree study he guided me on the technical aspects of research and ethical work related issues. He helped me build a practical approach to any kind of problem solving and his criticism helped me develop a keen understanding of my work, as well as greatly enhance my analysis skills. I would like to also thank him for the financial support he made available to me in the form of a Research Assistantship, which helped me continue my study and at North Dakota State University (NDSU).

I also want to thank the members of my graduate committee: Dr. Fardad Azarmi, Dr. Mariusz Ziejewski and Dr. Ekalak Khan, for allocating time from their busy schedules to serve on my committee. Their contribution was vital towards the completion of my research and thesis. I would like to thank Dr. Alan Kallmeyer, Chair of the Mechanical Engineering Department, as well, for his support and guidance and for offer of financial support he provided in the form of a Teaching Assistantship in the Mechanical Engineering Department at NDSU.

It is important to acknowledge the Air Force Office of Scientific Research (AFOSR) and the Army Research Office (ARO) for the financial support that made this research work possible.

TABLE OF CONTENTS

LIST OF TABLES

LIST OF FIGURES

1. INTRODUCTION

1.1. Interfacial properties between glass fiber epoxy matrix composite – background

The extensive use of glass fiber reinforced polymer matrix composites, or glass fiber-reinforced plastics (GFRPs) for industrial applications, has made research of this material very important. Properties of GFRPs such as its light weight, high strength and robustness are the reason it is in such demand. GFRPs are better compared to the carbon fiber reinforced polymer with respect to their less brittle nature and cost. GFRPs can be formed by molding processes which are easy and relatively cheap. GFRPs are used in boats, automobiles, water tanks, pipes, external door skins etc.

Individual glass fibers are stiff and strong axially, both in tension and compression. They are weak in the shear directions. A single glass fiber may buckle under compression which may make it seem weak in compression but it is actually the longevity of the fiber which makes it buckle therefore when the pressure is released the fiber returns to its original shape. If glass fiber bundles are arranged in a chosen direction (similar to making a piece of metal of equivalent shape and volume), the respective material becomes strong in that direction. GFRPs are, therefore, made of various layers of glass fiber bundles arranged in preferred directions in order to provide the overall composite strength and stiffness in a controlled manner.

The mechanical properties of GFRPs are dependent on the strength of the glass fibers that are used to reinforce the matrix and the bond strength between the fibers and the matrix. This bond strength influences the interface and its properties. The bond strength, and in turn the interfacial properties, determines the stress transfer phenomenon between the fiber and the matrix. The stress transfer phenomenon is responsible for the use of these composites for respective applications.

The effect of interfiber distance on the interfacial properties of glass fiber/epoxy matrix composites was studied by Moon [1] with the help of fragmentation tests. Their study showed that the interfacial shear strength of the composite kept decreasing with the decrease in the interfiber distance less than 50 μm. The interfacial shear strength reached a saturation point above this interfiber distance. Keusch et al. [2] exclusively used different sizings of fibers to determine the influence of the glass fiber/epoxy matrix interface on the microscopic and macroscopic properties of the composite. Single-fiber pullout tests were conducted by them to study the fiber-matrix adhesion. They determined that sizings had a significant effect on the interfacial properties. Thio et al. [3] in their findings pointed out those filler particles of glass fibers in polymer matrix showed higher rates of debonding when the bond strength between them was weak. Yeung and Broutman [4] studied the effect of the interface strength of the glass fiber reinforced epoxy and polyester matrix on the impact energy of the laminate. They observed that with increase in shear strength between the laminas, which was used as a means to determine the strength of the interface, the initiation energy for epoxy and polyester laminates increased. The total energy for the polyester laminate assumed a minimum critical value at which the interlaminar shear strength, below the total impact energy, increased with reduction in interlaminar shear strength, with failure mode identified to be delamination.

1.2. Cohesive zones – background

Cohesive zones are continuum based models which are used as an alternative to the Linear Elastic Fracture Mechanics (LEFM) model in studying the effect of the initiation and progress of cracks in numerous materials. The Cohesive Zone Model (CZM) was first proposed by Barenblatt [5, 6] for the aforementioned purpose, and later adopted by Dugdale [7], to

demonstrate perfect plasticity of materials. CZMs are suitable for explaining interface debonding because they adopt a micro-mechanical concept with the help of constitutive equations. Yan and Shang [8] applied CZM to successfully simulate the debonding of an interface between the fiber and matrix of a composite. Jayaram *et al* [9] showed the importance of the effect of stiffness, strength and separation progress on the stress transfer phenomena between the fiber and the matrix. The theory behind the principle of CZM is based on crack propagation being dependent on the critical strain energy release rate. Fiber-matrix interfaces are modeled as CZMs by presenting them as a very thin layer (sometimes infinitesimal or 2-D) enclosed between the two materials. The behavior of such interface is governed by specific traction-separation laws incorporating the continuum approach. CZMs have been applied by numerous researchers in their FE studies since its inception due to its micro-mechanical approach. Xu and Needleman [10] proposed another unique traction-separation concept based on an exponential curve. They studied growth of fast cracks in brittle materials in pioneering their model. Tvergaard [11] created a quadratic traction-separation law. Camacho and Ortiz [12] studied impact damage in brittle material with a linear traction-separation law. Guebelle and Baylor [13] developed a bilinear traction-separation based CZM for simulation of transverse cracks in the matrix of a composite.

Cohesive zones are, therefore, phenomenological models which are interpreted with the help of constitutive equations since they do not physically exist in nature. As discussed earlier, these models are extremely useful in simulating the mechanical behavior of interface debonding in composite materials. This section explains the implementation of a cohesive zone as an interface between any two bodies. Figure 1 shows the reference configuration and the current configuration of two bodies.

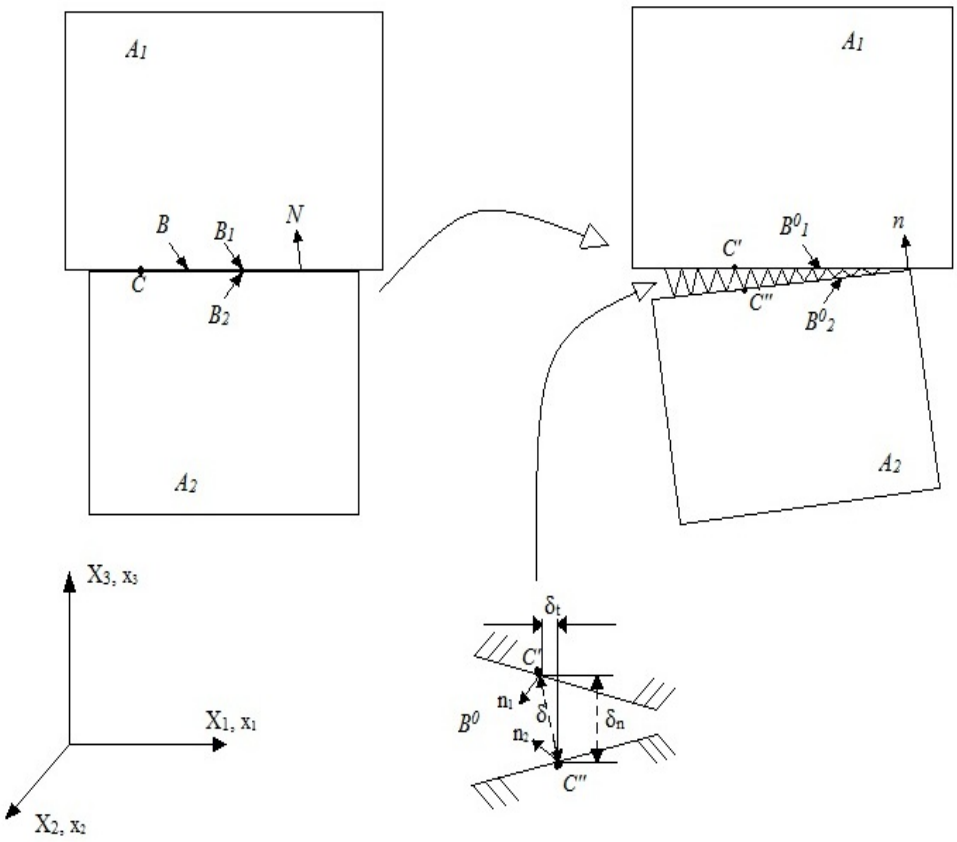

Figure 1. Representation of an interface as a cohesive zone model [14].

Two bodies A_1 and A_2 are assumed to share a common surface B when they are in contact with each other. B is considered to belong to both A_1 and A_2 correspondingly giving rise to B_1 and B_2. In the reference configuration $B = B_1 = B_2$. The reference configuration shows the cohesive zone as an infinitesimally thin 3-D entity with surfaces B_1 and B_2 before separation of the bodies. It can simply be taken as B. This is the interface between the two bodies. For a composite material, the fiber and matrix interfaces B_1 and B_2 belong to this fiber-matrix interface B [15].

A particle is considered to be at a position X in the reference configuration. In the current configuration this particle moves to position x after it undergoes a motion χ. The equation of

motion for this is given by $x_i = \chi(X_j,t)$ where t represents time. Unit normal N is used to define B. Subsequently, N_1 belongs to B_1 and N_2 belongs to B_2 with $N = N_1 = N_2$ before the separation. Upon separation n_1 and n_2 give the unit normal to the surfaces A_1 and A_2 as shown in Figure 1.

A 3-D structure is formed from the interface B when the bodies A_1 and A_2 separate. This formed region is not in harmony with the laws of continuum mechanics since the reference configuration cannot be used to define it. B^0 is the new interface domain. This domain now shares the surfaces shared by bodies A_1 and A_2 on either side. The interface in the current configuration is defined, therefore, by $B^0{}_1$ (shared between B^0 and A_1) and $B^0{}_2$ (shared between B^0 and A_2). The deformation of the interface causes the normal N to change to n_1 and n_2.

The constitutive equations of shear traction and shear separation, in terms of normal traction and normal separation, represent the interface domain B^0. It can be assumed that n_1 and n_2 are same for a narrow region. The traction vector for the interface is given by [15]:

$$T = \frac{\partial \varphi(\Delta)}{\partial \Delta} \tag{1}$$

With reference to Figure 1, the traction-separation behavior is governed by the following relations [15]:

$$T = \sigma n \qquad (\text{when } |\delta| < |\delta_{sep}|) \tag{2}$$

$$T = \sigma n = 0 \qquad (\text{when } |\delta| \geq |\delta_{sep}|) \tag{3}$$

where

T – traction on the surface

φ – potential of the interface

Δ – relative displacement of the interface

σ – stress tensor

n – normal to the surface

δ – separation

δ_{sep} – maximum separation

In the current context, researchers have used CZMs to observe the debonding phenomenon in glass fiber reinforced epoxy matrix during the machining of such composite materials [16, 17]. Fuchs and Major [18] illustrated how to determine the CZMs in glass fiber reinforced epoxy composites through an experimental procedure.

The exponential and bilinear CZMs were chosen to represent the interfaces in the respective studies of axial and shear loading. FE package ANSYS 12 has the capability to appropriately simulate the stress transfer phenomena in for both the CZMs.

1.3. Exponential cohesive zone model

Xu and Needleman came up with a constitutive model for their cohesive zone which was based on the theory of a potential $\varphi(\Delta)$. This potential is the amount of energy that is required to separate the planes across a relative displacement Δ [10]. The exponential CZM represents both the normal and the shear components of the traction-separation relationship simultaneously. The traction component and its derivatives are also continuous in nature for the exponential model as seen from the curve in Figure 2. From a computational point of view, this makes the exponential CZM more feasible than the other cohesive zone models. The stability for this model is derived from the assumption that the potential for the normal work of separation (φ_n) is equated to the potential for the shear work of separation (φ_t). This is given as [10]:

$$\varphi(\Delta) = \varphi_n - \varphi_n exp\left(-\frac{\Delta_n}{\delta_n}\right)\left\{\left[1+\frac{\Delta_n}{\delta_n}\right] exp\left(-\frac{{\Delta_t}^2}{{\delta_t}^2}\right)\right\} \quad (4)$$

where

δ_n – characteristic normal interface length

δ_t – characteristic tangential interface length

Δ_n – normal displacement jump vector

Δ_t – tangential displacement jump vector

The value of traction in this model increases with the increase in the separation of the surfaces, subsequently reaching a maximum value. After this the traction keeps decreasing, potentially approaching a zero value as seen in Figure 2. The nature of the curve is clearly indirect.

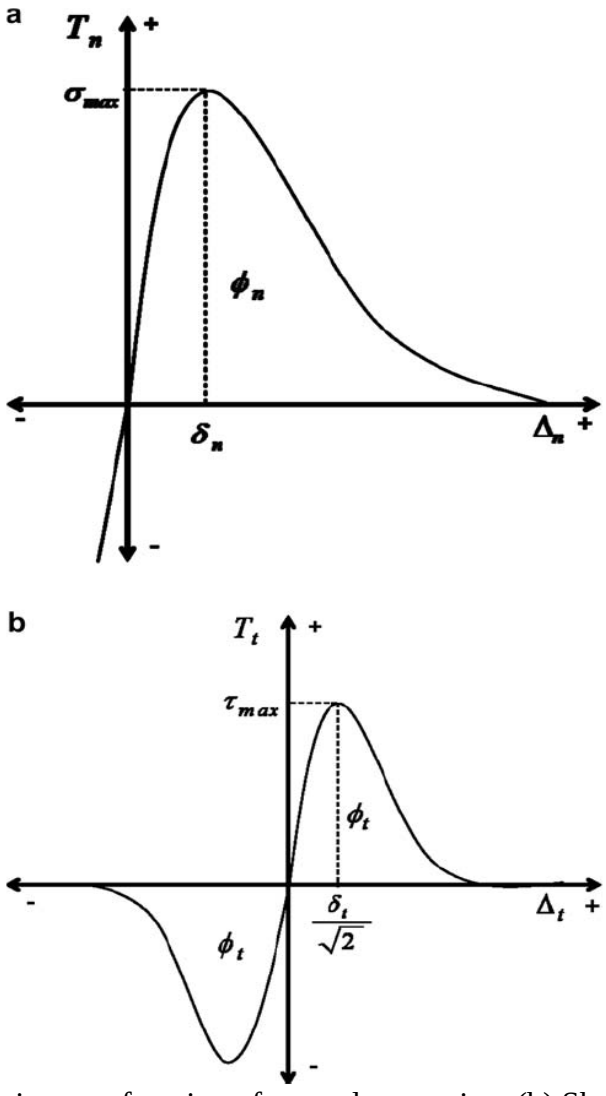

Figure 2. (a) Normal traction as a function of normal separation. (b) Shear traction as a function of tangential separation [10].

The interfacial traction values – T_n (normal traction) and T_t (shear traction); can be obtained from the following relationships [10]:

$$T_n = \frac{\varphi_n}{\delta_n} exp\left(-\frac{\Delta_n}{\delta_n}\right)\left\{\frac{\Delta_n}{\delta_n} exp\left(-\frac{{\Delta_t}^2}{{\delta_t}^2}\right)\right\} \quad (5)$$

$$T_t = \frac{\varphi_n}{\delta_n}\left(2\frac{\delta_n}{\delta_t}\right)\frac{\Delta_t}{\delta_t}\left\{1 + \frac{\Delta_n}{\delta_t}\right\} exp\left(\frac{\Delta_n}{\delta_n}\right) exp\left(\frac{{\Delta_t}^2}{{\delta_t}^2}\right) \quad (6)$$

The interfacial separation values - φ_n (normal separation) and φ_t (shear separation); can be obtained from the following relationships [10]:

$$\varphi_n = e\sigma_{max}\delta_n \quad (7)$$

$$\varphi_t = \sqrt{\frac{e}{2}}\tau_{max}\delta_t \quad (8)$$

where

e – exp(1) = 2.718

σ_{max} – interfacial normal strength

τ_{max} – interfacial tangential strength

The exponential CZM is applied to a representative volume element (RVE) to develop a preliminary FE model. This preliminary model is used to determine the feasibility of the use of a similar FE model in further accurate shear test models. The preliminary model serves the purpose of also showing the appropriate use of CZM in such an FE model.

1.4. Bilinear cohesive zone model

The bilinear CZM accurately predicts the shear mode delamination of the interface. Alfano and Crisfield [19] came up with this model in their work which forms the basis of the

bilinear CZM in ANSYS 12. The uncoupled model in their study is free of the axial forces and henceforth axial stresses.

An interface between the two bodies is considered to be of negligible thickness considering the dimensions of the overall geometry. The FE discretization of the interface, as such, is justified by effectively using elements which connect the two bodies but have zero thickness (considered before the delamination of the two bodies). In such a scenario, this interface can be imagined as a line. A linear element with 4-nodes (INT4) and a quadratic element with 6-nodes (INT6) are shown in Figure 3. (a) and (b), respectively.

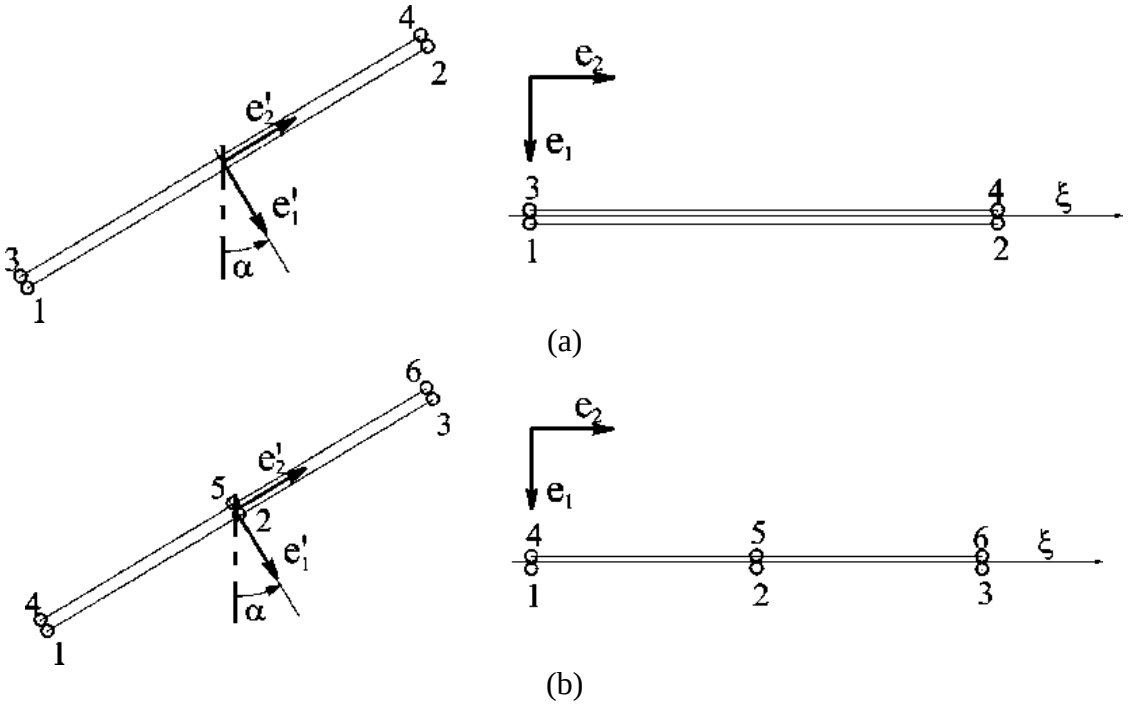

Figure 3. (a) Linear 4-node interface element. (b) Quadratic 6-node interface element. [19]

These elements are used to represent the interface. Since these elements are 2-D in nature, the stresses and strains in them will, in fact, present themselves as interface tractions and their corresponding relative displacements. A local reference system is established for each element which makes the relative displacements a vectorial sum of the traction mode 1 and sliding mode 2. The displacement is denoted as $\delta = (\delta_1, \delta_2)$ and the traction as $t = (t_1, t_2)$.

The displacement parameters can be referred to as a vector $p = [p_1, \ldots, p_n]$ where n represents the number of nodes (4, or 6) for the corresponding 4-noded, or 6-noded, element for convenience. This is according to the global reference system $\{e_i\}$ in Figure 3. The traction δ can be represented with respect to the local reference system $\{e'_i\}$, also shown in Figure 3. This gives the matrix B which forms the relationship between δ and p as [19]:

$$\delta(\xi) = B(\xi)p \tag{9}$$

Now B is dependent upon the movement of the element's rotation and is subsequently given by [19]:

$$B(\xi) = \sum_{i=1}^{n} B_i(\xi) \tag{10}$$

where

$$B_i(\xi) = \begin{bmatrix} \cos\alpha & \sin\alpha \\ -\sin\alpha & \cos\alpha \end{bmatrix} \tag{11}$$

Here $i = 1, \ldots, n/2$ and $\psi(\xi)$ is the value at ξ from the shape function at node i and $\psi_{i+n/2} = -\psi_i$.

The single mode delamination of the interface in the present model, corresponding to Mode 2 debonding, occurs when a tangential slip occurs between two surfaces. Figure 4 shows the relative traction-separation curve for the bilinear CZM. The equation for the given curve is represented by [19, 20]:

$$\tau_t = K_t \delta_t (1 - d_t) \tag{12}$$

where

τ_t – interfacial shear stress or traction

K_t – slope of the curve or the penalty stiffness parameter

δ_t – interfacial shear separation or relative displacement

d_t – debonding parameter

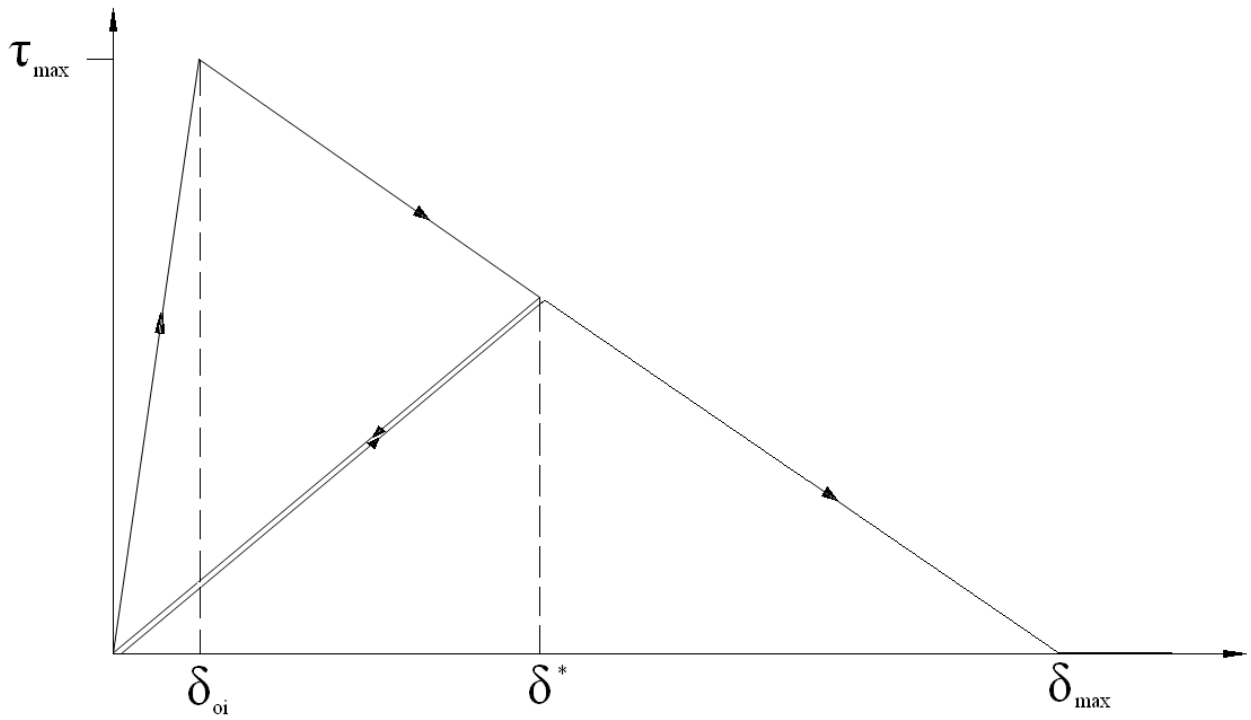

Figure 4. Relative traction-separation bilinear curve.

The debonding parameter for Mode 2 is given as follows [19]:

$$d_t = \left(\frac{\delta_t - \delta_{oi}}{\delta_t}\right)\left(\frac{\delta_{max}}{\delta_{max} - \delta_{oi}}\right) \tag{13}$$

The corresponding values of d_t are:

$d_t = 0$ when $\Delta_t \leq 1$

$0 < d_t \leq 1$ when $\Delta_t > 1$

where $\Delta_t = \delta_t/\delta_{oi}$

The debonding parameter is calculated on the assumption of isotropic behavior of the interface. The value of δ_t required for computation of d_t is obtained from 3-D stresses produced from the 2-D interface after debonding due to the shear stress state in the interface. This is given by [19]:

$$\delta_t = \sqrt{\delta_y^2 + \delta_z^2} \tag{14}$$

where δ_y and δ_z are the relative displacements in the corresponding tangential directions. The respective shear stresses in the tangential directions are given by [19]:

$$\tau_y = K_t \delta_y (1 - d_t) \tag{15}$$

$$\tau_z = K_t \delta_z (1 - d_t) \tag{16}$$

The critical fracture energy (G_{ct}) for the shearing phenomenon is calculated by [19]:

$$G_{ct} = \frac{1}{2} \tau_{max} \delta_{max} \tag{17}$$

where

τ_{max}– maximum shear stress in the interface just before failure

The phenomenon of G_{ct} is used from Linear Elastic Fracture Mechanics (LEFM) theory for the progress of the failure of the interface with respect to delamination in 1.17. The total energy in this process is thus calculated from the relationship in 1.17, although the assumption in LEFM of the energy released at each point being instantaneous is disregarded. This is due to the fact that G_{ct} in laminated composites is a characteristic property of the interface and does not depend on the geometry, or applied loads, in the composites. G_{ct} of interfaces can be measured by conducting Mode 2 delamination tests on specimens. The energy stored in the interface computed by G_{ct} is essentially the specific elastic energy (sometimes referred to as the critical energy) just before the delamination process is initiated as seen in Figure 5.

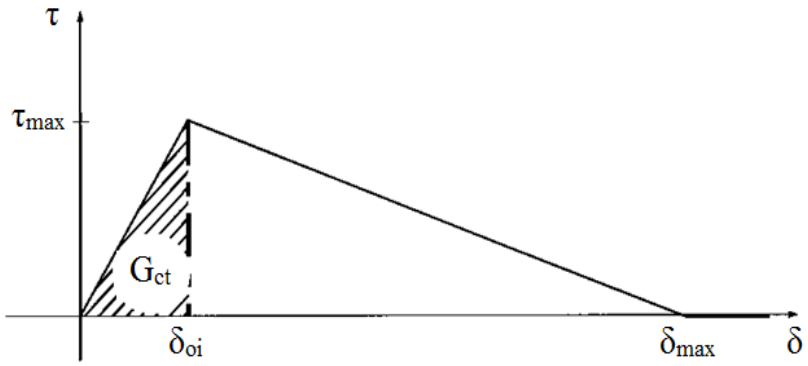

Figure 5. Specific elastic energy stored in the interface before delamination is initiated.

The start of the delamination process is the point where τ reaches its maximum value – τ_{max} and this is the shear strength of the interface. Once the value of τ_{max} is determined through experimental methods, δ_{max} can be obtained by the following relationship [19]:

$$\delta_{max} = \frac{2G_{ct}}{\tau_{max}} \tag{18}$$

The mesh of the interface for the bilinear CZM is directly related to τ_{max} (i.e. the computational effectiveness of the numerical problem is dependent on the shear strength of the interface). Higher values of τ_{max} require finer meshing while very low values of τ_{max} predict unsatisfactory results.

1.5. Periodic boundary conditions

Periodic boundary conditions (PBCs) are applied when the intention of the study is to predict and study the properties of the system in bulk and the properties are transmitted throughout the system in the same way. When the system under consideration is very large, compared to its surface, the surface effects of the system play little role in determining the mechanical properties of the system. Simulating such a large system is difficult, however, and hence, only a small portion of the continuous continuum is studied. Application of PBCs requires the effects of the surface, whether in the form of any load, or constraint, to be completely neglected. The body, or structure, under study is considered to be a small portion of the continuum. To implement the continuity of the small unit within the continuum PBCs are applied

For the purpose of this FE study, a repetitive composite unit cell model, far from the edge and within the volume of the material, is developed. This cell represents a small unit, which when repeated continuously in all the three co-ordinate directions, creates the entire continuum, or system, under study. In ANSYS, PBCs are applied by developing constraint equations which

are used to constrain nodes on opposite faces of the unit cell. Continuity of the unit cell, within the system, is achieved by constraining the displaced degree of freedom (DOF) of the nodes. The constraint equations are so developed to ensure identical deformation of opposite faces of the unit cell. A node at the geometric centre of each face is created to facilitate the application of PBC.

Three different constraint equation sets are developed for the purpose of applying PBC. Figure 6 shows the different faces of the RVE and the face numbers have been referred to accordingly. The first set of constraint equations are for the center nodes of opposite faces (faces 1 and 2, faces 3 and 4, faces 5 and 6) which undergo the same displacement in opposite directions. Next, separate equations are applied for the surface nodes, nodes on the edges of the unit cell and at the corners by constraining their DOF with respect to that of the center node, or their symmetric node pair, to ensure uniform deformation of the unit cell in the three co-ordinate directions. A unique coupling set is created for each specific coupling in order to avoid redundancy of constraint equations. In the constraint equations specifying PBC, U_i ($i=1,2,3$) represents displacement in *i-th* co-ordinate direction, C_i ($i=1,2\ldots\ldots6$) represents the center nodes on the *i-th* face, N_i and N_j represent node pairs on opposite faces, N_{ij} represents the nodes on the edges and N_{ijk} represents the corner nodes [21].

Constraint equations for the face center nodes:

$$U_i^{C1} + U_i^{C2} = 0$$

$$U_i^{C3} + U_i^{C4} = 0$$

$$U_i^{C5} + U_i^{C6} = 0$$

Constraint equations for all other nodes characterizing deformation of RVE:

Node pairs on face 1 and 2:

For all surface nodes on face 1 and 2 except those on edges and corners

$$U_i^{N2} - U_i^{C2} = U_i^{N1} - U_i^{C1}$$

For nodes on the edges 24, 13, 14, 23, 26, 15, 25, 16

$$U_i^{N24} - U_i^{C2} - U_i^{C4} = U_i^{N13} - U_i^{C1} - U_i^{C3}$$

$$U_i^{N14} - U_i^{C1} - U_i^{C4} = U_i^{N23} - U_i^{C2} - U_i^{C3}$$

$$U_i^{N26} - U_i^{C2} - U_i^{C6} = U_i^{N15} - U_i^{C1} - U_i^{C5}$$

$$U_i^{N25} - U_i^{C2} - U_i^{C5} = U_i^{N16} - U_i^{C1} - U_i^{C6}$$

For nodes on the corners 246, 135, 236, 145, 245, 136, 235, 146

$$U_i^{N246} - U_i^{C2} - U_i^{C4} - U_i^{C6} = U_i^{N135} - U_i^{C1} - U_i^{C3} - U_i^{C5}$$

$$U_i^{N236} - U_i^{C2} - U_i^{C3} - U_i^{C6} = U_i^{N145} - U_i^{C1} - U_i^{C4} - U_i^{C5}$$

$$U_i^{N245} - U_i^{C2} - U_i^{C4} - U_i^{C5} = U_i^{N136} - U_i^{C1} - U_i^{C3} - U_i^{C6}$$

$$U_i^{N235} - U_i^{C2} - U_i^{C3} - U_i^{C5} = U_i^{N146} - U_i^{C1} - U_i^{C4} - U_i^{C6}$$

Node pairs on face 3 and 4:

For all surface nodes on face 3 and face 4 except those on edges and corners

$$U_i^{N2} - U_i^{C2} = U_i^{N1} - U_i^{C1}$$

For nodes on the edges 46, 35, 36, 45

$$U_i^{N46} - U_i^{C4} - U_i^{C6} = U_i^{N35} - U_i^{C3} - U_i^{C5}$$

$$U_i^{N45} - U_i^{C4} - U_i^{C5} = U_i^{N36} - U_i^{C3} - U_i^{C6}$$

Node pairs on face 5 and 6:

For all surface nodes on face 5 and face 6 except those on edges and corners

$$U_i^{N6} - U_i^{C6} = U_i^{N5} - U_i^{C5}$$

The purpose of applying PBCs is to remove the concentrated effect of the point load applied on the unit cell in the x-direction. This is done since the unit cell has been modeled as small section of a larger homogenous continuum.

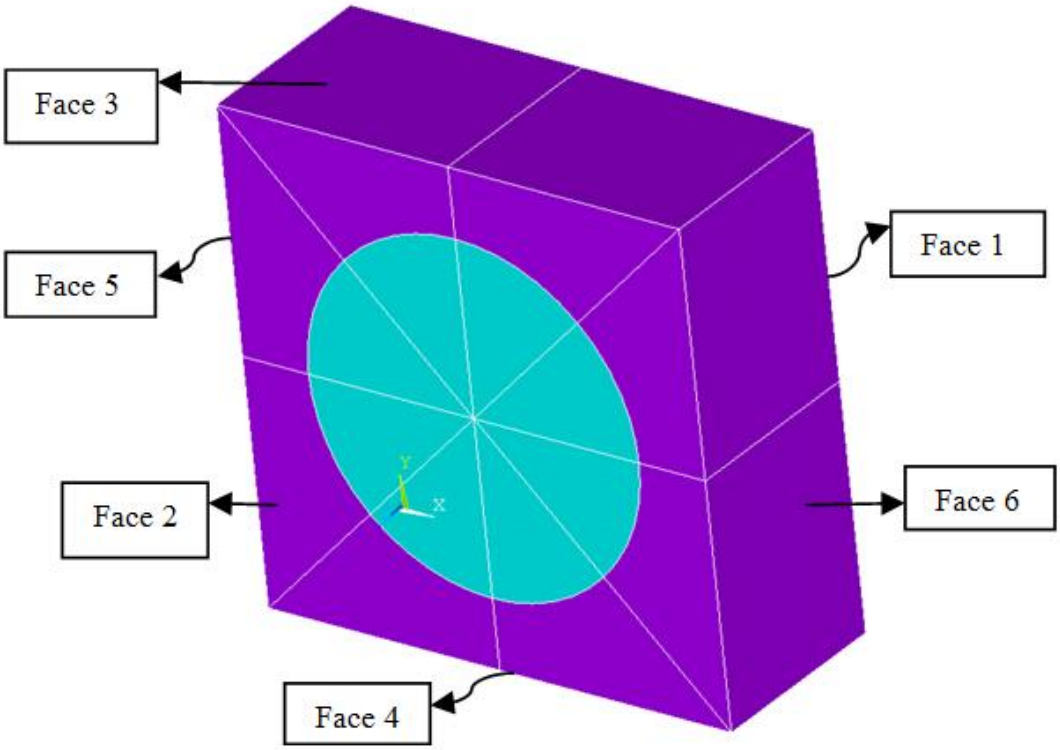

Figure 6. The faces of the RVE numbered in corresponding manner for creating the constraint equation sets.

This study aims in representing the results for the entire continuum by eliminating the criticality of the dimensions and the surface of the unit cell model alone. This has been achieved by simulating the model in such a way that if a force is applied on the larger continuum far away from the actual location of the cell, the force will be transmitted equally to all the unit cells irrespective of their location within the continuum. PBCs have been used to simulate the unit cell as a part of a larger continuum and to maintain the homogeneity of load within the continuum in the first FE model.

1.6. The pull-out test – background

A fiber pull-out test is the most common experimental technique used to determine the shear properties of the interface between the fiber and the matrix. Fiber pull-out tests, such as

fragmentation tests and droplet tests are some such tests. These aforementioned tests, however are disadvantageous in determining the real world behavior of the interfacial properties between the fiber and the matrix of a composite. This is due to the fact that the sample preparation of these tests does not take into account the residual stresses. Single fiber pull-out tests are also relatively simple in nature and specimen preparation is easier and less complicated. The specimen preparation is also cheaper and, thus, a greater number of tests can be conducted resulting in more reliable data.

Hampe and Marotzke [22] determined that the single fiber pullout test does not take into account the effect of neighboring fibers but give a detailed account of the debonding properties. They studied E-glass fibers in polystyrene and polycarbonate to determine properties such as interfacial fracture toughness (interfacial strength) and friction, along with the ductile nature of matrix and any residual stresses in them. They found that the E-glass fibers in polystyrene had 25% more interfacial strength for their pull-out tests than other such tests. E-glass fibers in polycarbonate had similar features in interfacial strength, along with the force-displacement readings showing ductile behavior of the matrix.

Zhandarov et al. [23] conducted single fiber pull-out tests to determine the effect of different diameter lengths on the interfacial bond strength and, consequently, the load transfer between glass fibers and polymer based matrices. Interfacial shear strength (τ_{max}) formed the basis of characterization in their study. This parameter was unaffected by the fiber diameter. It was observed that the release rate of critical energy (G_{ct}) was consistent with the constant fiber diameter. Their study showed that when the fiber diameter was increased, the release rate of G_{ct} decreased. The release of G_{ct} was more pertinent to the specimen geometry than τ_{max} with respect to the damage of the interface beginning. Overall it was determined that single fiber pull-out tests

were an appropriate tool to characterize interfacial properties in glass fiber polymer based matrices.

DiFrancia et al [24] compiled an extensive literature review on pull-out tests for different fiber-matrix composites including glass fiber epoxy matrix. In general, they interpreted that the shear stress of the interface between the fiber and the matrix at the onset of the debonding could be found through the release rate of G_{ct}. They also discovered that when the debonding length was at a certain value, the crack propagation in the steady-state occurred in such a manner that the frictional forces were relatively constant and were also at a maximum for that critical length of the fiber.

Tsai and Kim [25] tested glass fibers with a gold-palladium coating in an epoxy matrix to determine any difference in behavior of the interfacial strength and crack advancement (interfacial failure) from uncoated fibers by pull-out tests. The uncoated fibers showed an intense increase in interface strength with sliding mode interface failure. This was negated when the gold-palladium coating was introduced. They found that this increase in interface strength was due to the mode of failure being sliding mode debonding.

1.7. Research objectives

The initial model was built to take into consideration the effects of the axial loading conditions in such a manner so as to demonstrate the debonding phenomena as close to reality as possible. This was achieved with the help of PBC. The effect of PBC is intended to show how the debonding is replicated in the overall composite. The exponential CZM was applied to the initial model since the interfacial stresses and displacements in the normal direction would also take into account the effect of shear forces in the interface.

Objectives of the first FE model:

1. To create an FE geometry model, to show the debonding phenomenon in glass fiber epoxy matrix composites when a transverse load is applied.
2. To give insight into the debonding of the aforementioned model with the interface represented by an exponential CZM.
3. To study the current model and eliminate inefficiencies for creating a model depicting Mode 2 debonding.

Pull-out testing is performed on E-glass fiber and 8063 epoxy matrix composite material specimens to mainly determine interfacial properties which can be further used in an FE model. It is expected that these properties would aptly reflect the stress transfer of the interface in the FE model with the Mode 2 debonding phenomenon in the composite material.

Objectives of pull-out testing:

1. To find an appropriate embedding length of the fiber in the matrix that corresponds to clean fiber pull-out i.e. no matrix cracking, or fiber breakage (fiber failure), at the point of debonding (interfacial failure).
2. To investigate interfacial properties for Mode 2 debonding in E-glass fiber epoxy matrix composite material specimens.

The second FE model was to be built keeping in mind the real world pull-out testing performed on the composite and the mode of failure through which it was to undergo. The model needed to predict the shear stress transfer corresponding to the mode of failure.

Objectives of the second FE model:

1. To create a model for predicting the stress transfer phenomenon between the fiber and the matrix of the composite material.

2. To investigate the Mode 2 debonding phenomenon in the created model in accordance with the interfacial properties obtained from pull-out testing.

As mentioned in 1.6, fiber pull-out test takes into account some of the important factors required to appropriately model the interfacial properties in a continuum based study. The interfacial properties obtained from the pull-out testing were used in FE modeling with the help of CZM. The pull-out test is essentially Mode II debonding and it was demonstrated in [15] that a bilinear CZM could be used to study this debonding phenomenon through FEA. The interfacial properties between glass fiber and epoxy matrix derived from pull-out testing was thereby used in the FE study.

1.8. Applications of research in literature

Wool [26] explored the importance of interfaces with regards to the interface fracture strength of thermoplastic composites. They used a microscopic deformation mechanism which involved analyzing bond rupture. This mechanism determines the strength of the interface based on the fact that the interface uses a known amount of energy to deform. This method is used to evaluate the fracture energy of symmetric interfaces of polymer composites formed when these composites are manufactured by lamination, tow placement and welding.

Baillie et al. [27] did an extensive study on the bonding potential of interfaces of fiber surfaces. They did not find any data which could explain the adhesion or real bonding of fiber surfaces. They found that previous literature could only support interfaces as a physical entity with a distinct size. The interface does not have a consistently measureable feature since the interface location and properties keep changing when the fiber surface is treated. CZMs are an

approach which mimics interfaces in a way where they have an infinitesimal size and the energy of the interface is taken into account.

Tenhaeff et al. [28] showed the relevance of interfaces in composites of solid polymers and glass electrolytes through modeling and electrochemical mechanical characterizations. Solid state batteries can replace Li-ion batteries and they have the advantage of being safer because they are not composes of flammable organic liquid electrolytes. Dry polymer, glass and ceramic can act as solid electrolytes. These solid electrolytes are seen to have mechanical properties comparable to Li anode. They demonstrated the effect of interface on conductivity and mechanical properties by arranging layers of inorganic and polymer electrolytes together. The inorganic layers were made of lithium phosphorus oxynitride (Lipon). Li conductivities were characterized by deposition of thin films of Lipon and then fabricating polymer electrolytes over Lipon by spin coating. Their observations through electrochemical impedance spectroscopy revealed that interfacial resistance was the dominating factor in the bilayer structure.

Fraunhofer Institute for Manufacturing Technology and Advanced Materials IFAM, Bremen, Germany [29] have found through their R&D activities on adhesive bonding technology that the combination of materials through different joining techniques yields multifunctional products with lightweight design and decrease in size. Their GFRPs specifically are used in shipbuilding and wind turbines. The institute has been able to analyze surface pre-treatments (for example – use of release agent residues on strength of bonded joints) through their interface research. Other applications of their interface research include preventing galvanic corrosion and electrical insulation of materials.

Multiscale Computational Mechanics Laboratory in Vanderbilt University [30] is developing nanoscopically-informed mechanical interfacial models through which they can build

molecular-level materials. This would mark a shift in the traditionally engineered materials to intelligent composites.

2. EXPERIMENTAL

2.1. Sample preparation

Interfacial failure can be interpreted as clean fiber pull-out from the matrix in terms of pull-out testing. Clean fiber pull-out corresponds to a fiber specimen remaining intact in terms of the complete embedded length in the matrix, as well as the matrix not undergoing any cracking when the fiber is completely out of the fiber. The fiber bundles to be formed were to be, therefore thick enough to withstand the pull-out force and not undergo any breakage (fiber failure) before interfacial failure. They were also not to be so thick as to cause matrix cracking in the specimen. This thickness was achieved by testing various bundle sizes and impregnation depths. The tests dictated that the impregnation depth be small to achieve pullout.

It was found that three individual E-glass fiber strands combined together to form a fiber bundle was optimal for an impregnation depth of 1.63 mm. The fiber bundles were pulled with a threading needle through a clean Neoprene rubber gasket. The fibers were pulled sufficiently so as to be protruding from the gasket and then trimmed to the required length. These were then kept on a rack of level height and droplets of the resin were applied on the upper surface with the fibers protruding to fully encapsulate the fibers.

Huntsman 8603 RenInfusion™ epoxy resin system was used to prepare the matrix. RenInfusion™ 8603 (resin) and Ren® 8603 (hardener) is a two-component epoxy system for applications in advanced composites. It is a low viscous epoxy system which is mixed 100:15 parts by weight of resin:hardener and has a curing time of 24 hours. After curing, a spit shot weight (fishing weight) was used to clamp the fibers together and align them unidirectionally at the bottom. The dry end clamped together was then trimmed and potted in the resin.

2.2. Testing

The cured samples were then removed and tested on an INSTRON load frame, model 5567 (Norwood, MA, USA) carrying a 2 kN load cell with a rate of displacement of 0.5 mm/min [14]. Specimens that underwent premature fiber failure, or matrix failure, were discarded. Interfacial failure was only achieved once the critical stress value was reached. The samples which exhibited successful pullout were then examined under a ZEISS Axiovert 40MAT microscope fitted with a Jenoptik Progres C10 3.3 megapixel CCD digital camera. They were processed using iSolution DT imaging software to determine the perimeter of the contact between the fiber bundles and the epoxy resin and also the surface area of the fiber from the top. A modified Kelly-Tyson equation was used to determine the shear strength of the interface, τ_{max} [31]:

$$\tau_{max} = \frac{F_{max}}{CL_e + A} \tag{19}$$

where

F_{max} – maximum load at pull-out

C – fiber bundle perimeter

L_e – fiber embedded length

A – cross-sectional area of the fiber as measured from the top

3. FINITE ELEMENT MODELING

3.1. Geometry, material properties, meshing and interfacial properties of the first FE model

Geometry – A geometrical model of the composite material was constructed in the FE package ANSYS 12 where a circular fiber was enclosed by a square matrix as shown in Figure 7. The fiber bundle is the green circular figure in the middle. The purple figure surrounding the fiber bundle is the matrix. The zero thickness layer between them is the interface. The length (and breadth) of the model was 100 mm and the width of the model was 40mm. The overall dimensions of the geometrical model were taken in such a manner so as to maintain a fiber volume ratio of 40%. The radius of the fiber bundle was, therefore, 35.68 mm.

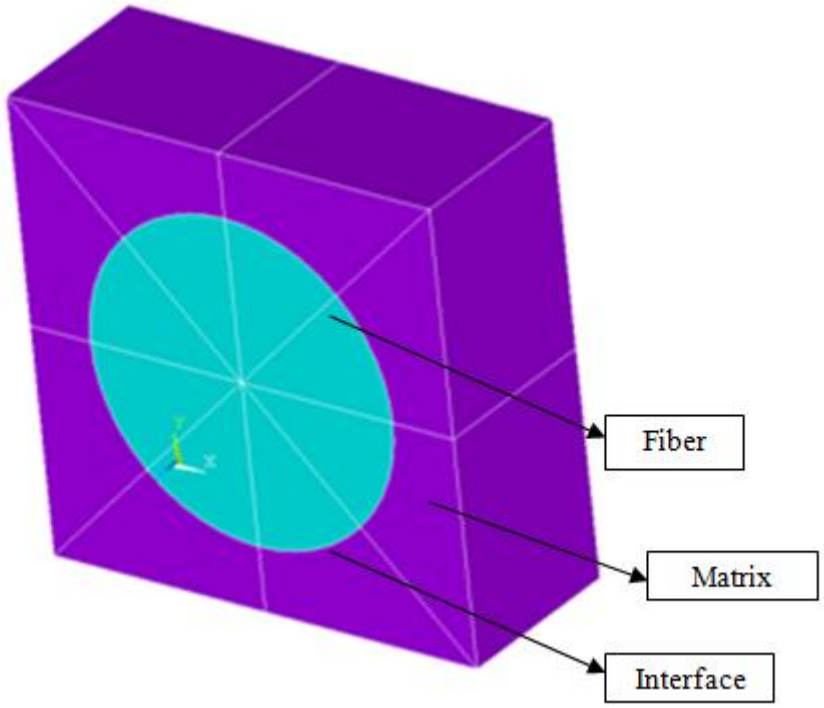

Figure 7. Geometric model of the composite material for the first FE model.

The geometric model shown in Figure 7 was chosen based on the simplicity of its construction and reliability of results in models where a circular fiber was enclosed by a rectangular/square matrix [21]. The fiber volume ratio chosen was optimal for observation of the

stress transfer patterns in the interface. Element SOLID 45 from the ANSYS 12 element library was used to construct the entire model and maintain uniformity of the structure. The make-up of a single SOLID 45 element is shown in Figure 8 [20]. The element was simple enough to project the stress transfer between the layers and yet accurate enough to give the proper mesh size. Figure 8 shows the locations of the nodes and the direction of the coordinate system for this element. Pressure loads were applied on the element in the form of surface loading with a positive value forcing the surface of the element in and a negative value forcing the surface of the element out. The element had 8 nodes and the material properties were orthotropic in nature. The respective surface loads on the element are shown by circled numbers in Figure 8.

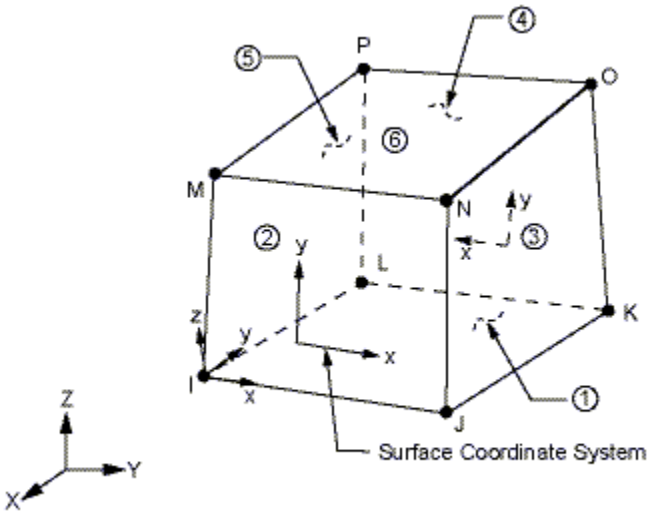

Figure 8. Element SOLID 45 geometry [20].

This element was chosen for the following reasons:

1. Interfacial stress transfer calculations take a lot of time to solve, being CPU extensive. The chosen element requires less time to solve for stiffness formation and achieves faster stress/strain calculations than other comparable elements in the same class.
2. The interfacial stress-displacement calculations are highly non-linear in nature and nonlinear convergence of the chosen element is generally a positive factor.

3. The element has the advantage of being free of volumetric errors mainly caused due to plasticity or other incompressibility issues in materials.
4. SOLID 45 element history is $1/7^{th}$ as much as it should be if full integration is applied due to its uniform reduced integration method.

Material properties – Both the E-glass fiber and epoxy matrix are considered linear elastic and isotropic in nature. The material properties for the fiber and matrix are given below.

Table 1. Mechanical properties of E-glass fiber and epoxy matrix used in the first FE model [16].

Material	*Young's modulus (MPa)*	*Poisson's ratio*
E-glass fiber	72000	0.22
Epoxy matrix	3100	0.33

Meshing – A mesh size of 4 units for each quarter of the structure was applied to both the fiber and the matrix with respect to the length and breadth of the model. The mesh along the width of the model was 2 units. This can be seen in Figure 9. The mesh size along the length and breadth of the model was finer compared to the width since axial loading was applied to the geometry. Normal interfacial stresses needed, therefore, to be observed on the front/back faces of the model. This mesh pattern in the initial study was chosen since a coarser mesh would not yield an accurate enough result to predict the interfacial stresses, or the stress transfer, between the matrix and the fiber. A finer mesh than the present one was observed to cause problems with respect to convergence in the Newton-Raphson method at the onset of debonding due to the combination of PBC and the exponential CZM. The overall mesh pattern shown in Figure 9 was constructed in a unique symmetrical way so that it could properly display the resulting stresses in the body uniformly, as well. Non-uniform stresses caused by random meshing represented inaccurate results.

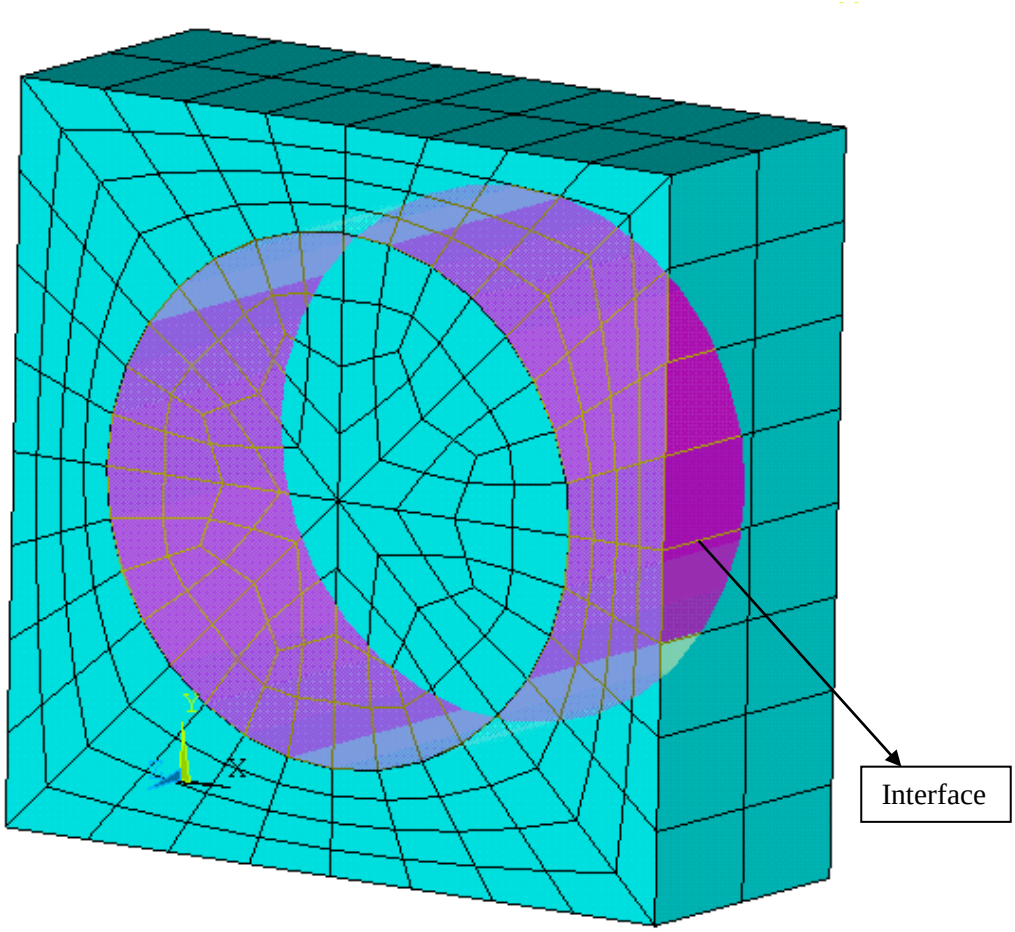

Figure 9. Mesh applied to the first FE model with the zero thickness interface and its elements (interface in purple).

Interfacial properties – The interface shown in Figure 7 was integrated within the FE model with the help of the exponential CZM discussed earlier in section 1.3. There was a total of 64 elements in the interface. All the elements had zero thickness and this was visible in Figure 9.

The parameters required to define the exponential CZM in the present context are the surface potential (φ) or the energy required to separate the surfaces, maximum value of normal traction (σ_{max}), and maximum value of shear traction (τ_{max}). The normal surface potential is equal to the shear surface potential. These values are as follows [16]:

$\varphi(n) = \varphi(t) = 50$ N/m

$\sigma_{max} = 160$ MPa

τ_{max} = 34 MPa

The normal separation can be found by the following relationship [10]:

$$\varphi_n = e\sigma_{max}\delta_n \tag{20}$$

The shear separation can be found by the following relationship [10]:

$$\varphi_t = \sqrt{2e}\tau_{max}\delta_t \tag{21}$$

The interface defined by the exponential CZM is composed of INTER 205 elements from the ANSYS 12 element library. This particular element is the one that is compatible with the SOLID 45 elements of the fiber and matrix in the composite structure. INTER 205 is an 8-noded 3D interfacial element which simulates the debonding phenomena between two surfaces. The nodes are coincident upon each other in the beginning with each node having three DOFs, namely translational movement in x, y and z directions. The geometry of the element with the nodes and the DOFs are shown in Figure 10.

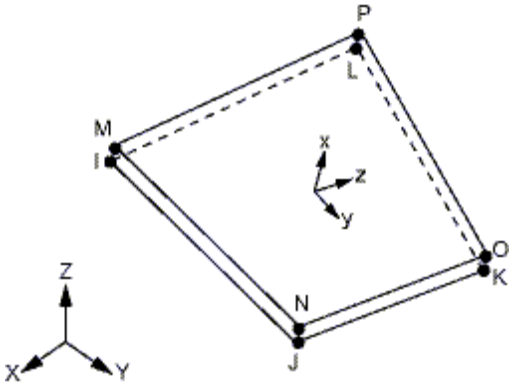

Figure 10. INTER 205 element from the ANSYS 12 element library showing the nodes initially coincident on each other and having translational movement in the coordinate directions [20].

3.2. Boundary and loading conditions for the first FE model

The load case considered for the model in context was a single transverse loading. This loading was applied on the model in the form of a single concentrated force on the center node of a surface which was parallel to the y-axis in the x-direction of a coordinate system. This same

loading scenario was equally projected on the opposite surface, or side of the structure, to which the load had been applied due to implementation of PBC. A singular concentrated tensile force in the axial direction was applied on the central node of face 6. This loading condition can be seen in Figure 11. The red arrow indicates the load applied on the body. The debonding of the interface in the normal direction is aptly portrayed by this loading scenario. Application of PBC enables the loading to be applied in both the directions uniformly with equal and opposite effect. The nodes in the structure are constrained by equations in such a way that the effects of stress are transferred throughout the continuous medium.

PBCs are important to determine the behavior of the overall composite with reference to the interface between the fiber and the matrix. The interface will behave in the same way wherever the bonding between the fiber and the matrix exists. Therefore the RVE constructed here with the loading and boundary conditions showed how the interfacial failure occurred in the overall composite material. The normal interfacial separation on both sides of the fiber can effectively be modeled with PBCs applied to the RVE. If there is no PBC then the direction of loading does not appropriately reflect how the transverse loading is propagated throughout the composite material. However in the case of a non transverse loading (as shown later in Mode 2 debonding), PBCs do not need to be applied since the shear stresses and strains come into effect which are not propagated through the composite in the same way as in the case of transverse loading. This loading resulted in the development of transverse stresses in the x-direction. The present loading projected failure in composites with respect to normal interfacial debonding. The boundary conditions for the model needed to be such that they prevented rigid body motion, or they prevented the free movement of the body in the direction of force application.

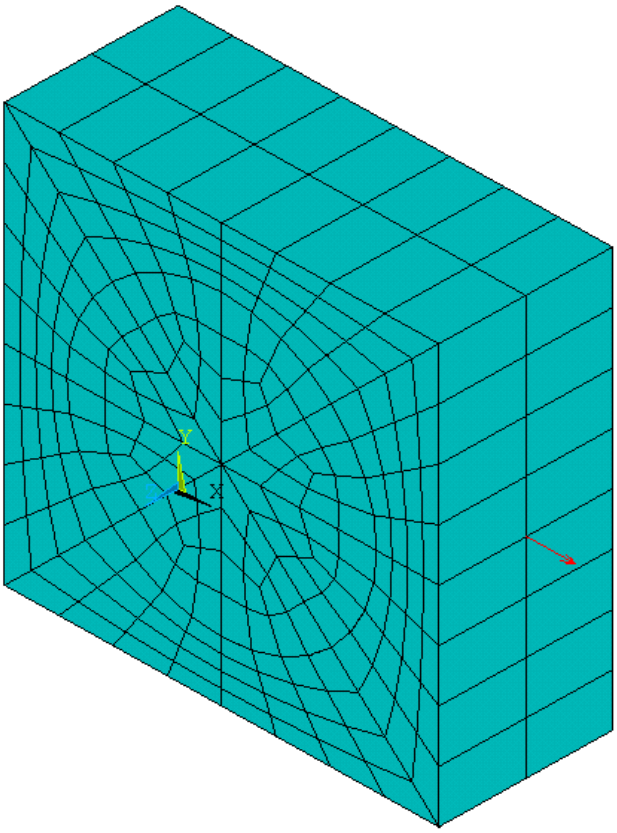

Figure 11. Transverse loading (red arrow) applied on the central node of face 6.

Rigid body constraints were applied, therefore, as follows:

1. fixing the center node of the body in all the three coordinate directions;
2. fixing the center node on face 1 in x and y coordinate directions;
3. fixing the center node on face 2 in x and y coordinate directions; and
4. fixing the center node on face 3 in x and y coordinate directions.

The transverse load application on the face of the unit cell represented a force applied on the continuum in the transverse direction away from the surface of the unit cell. The application of PBC enables the force to be transmitted continuously through the continuum on the transverse face of the unit cell. Interfacial debonding was initiated by pulling the transverse face of the matrix on either side away from the fiber and hence FE solution for the response of the unit cell of the load is a representative of the response of the continuum for the same loading.

3.3. Geometry, material properties, meshing and interfacial properties of the second FE model

Geometry – The second FE model was built mainly for the computation of shear stresses in the interface when there was Mode 2 debonding between the fiber and the matrix. The stress transfer between the fiber and the matrix of the composite material also needed to be computed as an effect of the shear debonding. The geometry of the second model was similar to the first model in all respects. The length, breadth and width of the geometry were the same as the first FE model. The second model is shown in Figure 12 with the fiber, matrix and interface distinguished from each other. This was done to obtain a fiber volume ratio at 40% since the interfacial shear stress patterns could best be observed at this value. The interfacial properties obtained from the pull-out tests were to be directly implemented in this model. The area of concern for building the second model was, therefore, the application of the interface. It is to be noted here that the area under a force-displacement curve, obtained from experimental results, is the measure of the stored energy required for complete debonding of the fiber from the matrix. This area depends upon the following three factors:

1. embedded length of the fiber bundle;
2. surface area of the fiber bundle; and
3. perimeter of the fiber bundle

A change in these three parameters proportionally changes the area under the curve as seen in the literature. If the parameters are kept constant, then the area under the curve would ideally remain the same along with the energy required for debonding. Thus, the parameters (characteristic strength and characteristic separation) required to define a cohesive zone would be independent of the parameters that control the area under the force-displacement curve. The fiber

volume ratio would, in turn, be unaffected, therefore, as long as the area under the curve remains the same.

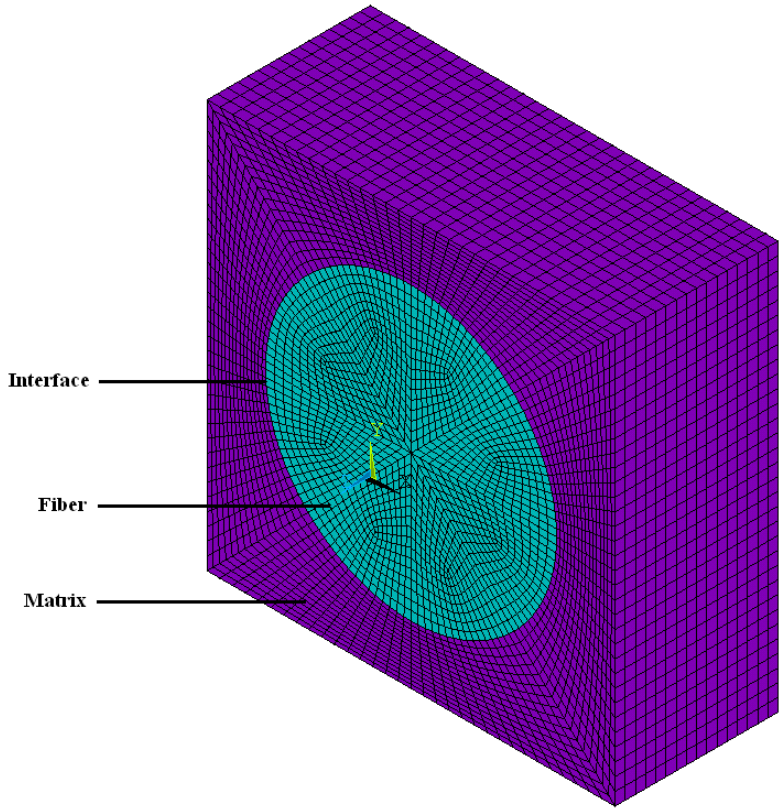

Figure 12. Geometric model and mesh size shown for the second FE model.

Material properties – The material properties of the fiber and matrix had values close to those in Table 1 but these values slightly differed since they were obtained for the materials used in the pull-out tests. Both the E-glass fiber and epoxy matrix are considered linear elastic and isotropic in nature. These are shown in Table 2 [16].

Table 2. Mechanical properties of E-glass fiber and epoxy matrix used in the second FE model.

Material	*Young's modulus (MPa)*	*Poisson's ratio*
E-glass fiber	72500	0.22
Epoxy matrix	3021	0.33

Meshing – A uniform mesh size of 16 units per quarter of the body was chosen for both the fiber and the matrix along the length and breadth. The mesh along the width was 16 units, as

well. The mesh size selected depended upon two factors: 1) stress transfer from the fiber to the matrix through the interface, and 2) the stress pattern to be observed in the interface. To accurately predict these two phenomena, a mesh size was chosen which was not so fine as to cause convergence problems and also required reasonable time to solve the iterations in ANSYS [20]. This mesh size is shown in Figure 12. The same unique mesh pattern used in the first model is used here, as well, but in a much finer manner.

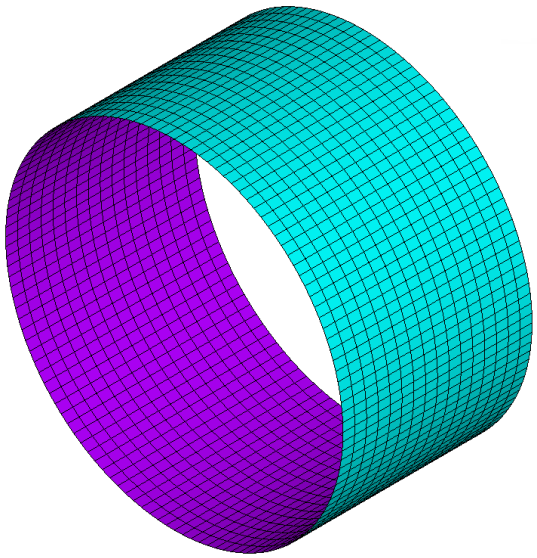

Figure 13. The zero thickness bilinear cohesive zone integrated between the fiber and the matrix.

Interfacial properties – The interface for the second FE model is shown in Figure 13. This was incorporated into the model with the help of a bilinear CZM. The total number of elements in the cohesive zone was 2048 and they were all zero thickness. For Mode 2 debonding, the cohesive zone was defined using the following parameters:

1. the work of shear, or tangential, separation G_{ct} (this was calculated from the area under the force-displacement curve obtained from pull-out tests just before the onset of interfacial failure);

2. the shear, or tangential, traction (characteristic shear strength of the interface) τ_{max} (this was also obtained from the force-displacement curve just at the point of interfacial failure); and
3. the shear, or tangential, separation value (characteristic shear interfacial separation) at which complete debonding took place δ_{max}.

The first two parameters were computed from pull-out tests while the third parameter in the list is computed from equation 18 discussed in section 1.4. The bilinear CZM was made up of contact elements from the element library of ANSYS 12. These were CONTA 174 and TARGE 170 elements which were used in conjunction with each other. The CONTA 174 elements were applied to the surface of the fiber bundle while TARGE 170 elements were applied to the matrix surface. These contact elements are to be used along with the structural element SOLID 45. The stress transfer in the interface took place in a way that it was transmitted from the body, where the stress was applied, to the body where it was not. CONTA 174 represented the deformable surface to the 3-D target surface and had the same geometrical configuration as the solid element (in this case SOLID 45) with which it was connected. The contact surface elements simulated the debonding phenomena for interfacial delamination. Figure 14 shows the CONTA 174 elements before and after deformation.

The TARGE 170 elements were paired with CONTA 174 with shared sets of real constants which transferred corresponding motion and deformation to the target body such as the translational motion previously described. The behavior of TARGE 170, with respect to CONTA 174, is shown in Figure 15.

The two parameters of the bilinear cohesive zone – characteristic interfacial shear strength (τ_{max}) and characteristic interfacial shear separation (δ_{max}) are obtained from pull-out

testing: τ_{max} = 13.349 MPa; δ_{max} = 4.216 mm. These values are discussed in more details in the experimental results section namely section 4.2.

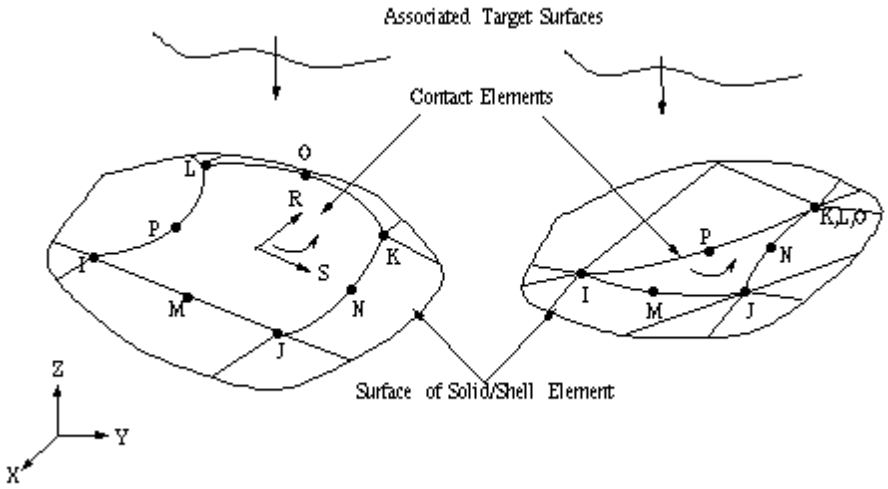

Figure 14. CONTA 174 elements displayed as 8-noded elements deforming to form 6-noded elements depending upon the shape of the underlying element [20].

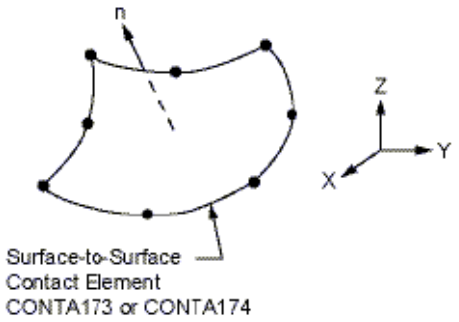

Figure 15. TARGE 170 behavior for corresponding deformation of CONTA 174 [20].

3.4. Boundary and loading conditions for the second FE model

The boundary conditions for the model were set up in such a way so as to mimic the pull-out test conditions in the experimental set up. The matrix was constrained in all three coordinate directions and on all the outer surfaces except the bottom one. The boundary conditions are shown in Figure 16. The coordinate directions are shown by the three triangle like figures.

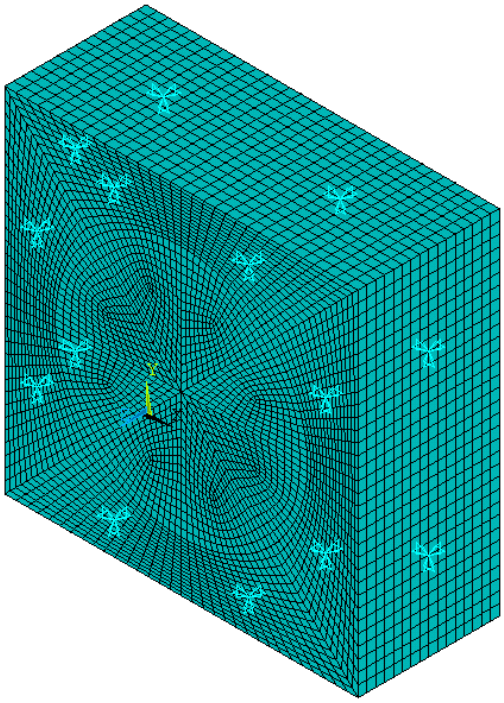

Figure 16. Boundary conditions showing the composite structure constrained in all three coordinate directions for all the matrix surfaces except the bottom one.

A uniformly distributed pressure value was applied on the upper surface of the fiber to simulate the force with which the fiber was pulled over a given cross-sectional area during the pull-out test. The loading scenario is demonstrated in Figure 17 where the red lines over the elements show the application of the loading pattern as a uniform value of pressure. For further references in this study, therefore, this pressure value will be referenced as the pull-out load/loading.

The pull-out loading conditions were mimicked in the boundary conditions of the FE study. This was done in the following way – a simplified model of the pull-out test was developed to co-relate the experimental and FE modeling. A_1 and A_2 in Figure 1 were assumed to be glass fiber and epoxy matrix respectively. Both were considered to be purely elastic and connected by interfaces. B^0 in Figure 1 was modeled by discretized FE interfacial elements governed by traction-separation laws, with the help of T-δ relations as explained in sections 1.2

and 1.4. If the pull-out load *F* applied in the experimental test moved the fiber inside the matrix by a distance of ΔL then a relationship between the F-ΔL and T-δ relationships can be established.

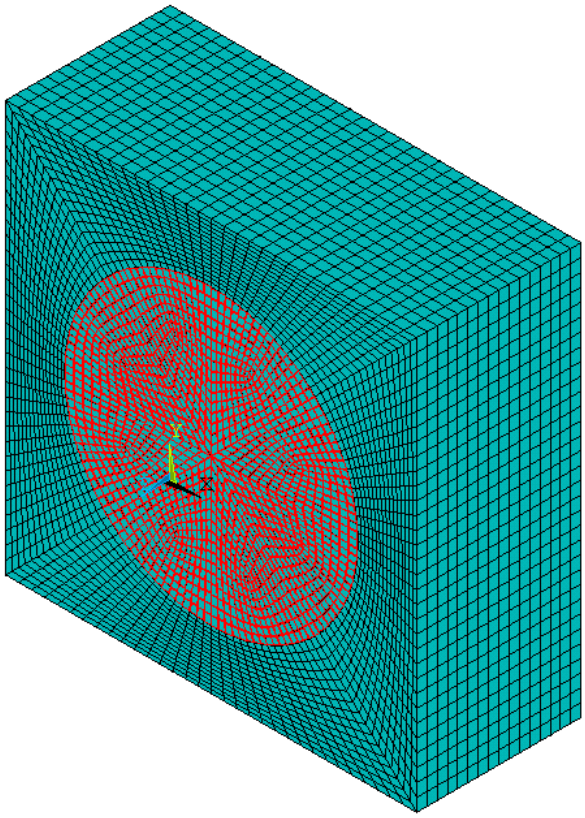

Figure 17. Uniform pressure loading applied on the top of the fiber shown by the red lines over the element traces.

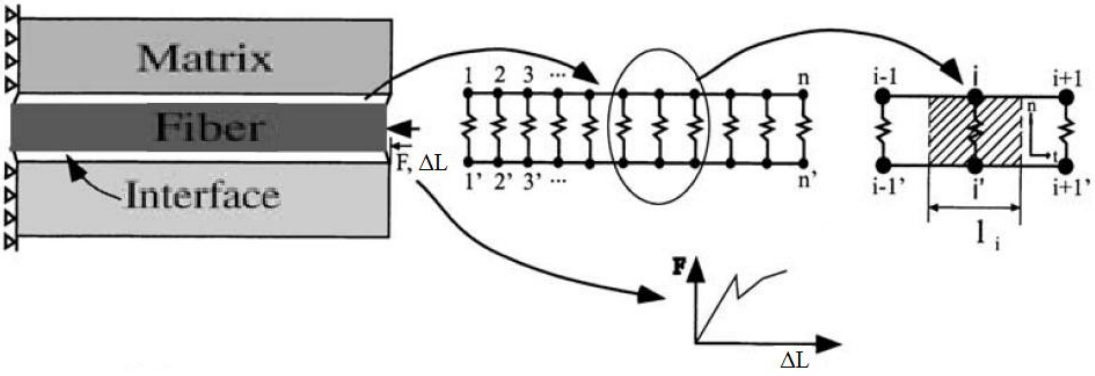

Figure 18. Free body diagram of the cohesive zone elements where springs represent the interface and the F-ΔL curve of the interface between the matrix and the fiber from the experiment [15].

The cohesive zone elements are simplified as non-linear springs as shown in Figure 18. The FE interface is made up of nodes which are assumed to be connected as springs at {1, 1′}, {2, 2′}, ... , {n, n′}. These nodes are located in the fiber and the matrix before the application of the load. Let T be the traction at spring i after a load F is applied and let f be the shear force represented by [15]:

$$f_i = \Pi d T_i l_i \tag{22}$$

where:

d – fiber diameter

T_i – average shear traction in the region of spring $(i - (i - 1))/2$ to $(i + (i + 1))/2$

l_i – axial length of the region

The shear separation of the springs i is governed by the T-δ relationship. The equilibrium of force gives us [15]:

$$F = \sum_{i=1}^{N} f_i \tag{23}$$

For a bilinear CZM when $\delta < \delta_{max}$; and assuming the matrix is still intact (as was the case in the experiment till debonding); for i^{th} spring we have $T_i = k_i\delta_i$ and $f_i = (\Pi\delta_i l_i)k_i d$ and therefore [15]:

$$F = \Pi d k_i \sum_{i=1}^{N} \delta_i l_i \tag{24}$$

It is known that the effective length of the spring remains constant; hence the complete length is expressed as a linear combination of each spring. Again, we also have [15]:

$$\sum_{1}^{N} \delta_i = \Delta L \tag{25}$$

From equation 22, 23, 24 and 25 we get [15]:

$$F = K'\Delta L \tag{26}$$

where K' – the slope of the curve from the pull-out test. This F-ΔL curve is shown in the in Figure 18. Thus the F-ΔL curve for the experiment corresponds to the T-δ curve for CZM shown in Figure 5.

The second model represents a FE simulation of the pull-out experiment. This model is not considered to be a part of continuum but is a representation of the actual fiber embedded in the matrix. The pull-out load was to be applied in only one direction on the fiber and was not to be transmitted along the length of the fiber. The surface of the fiber on which the load is applied experiences stresses which reduce along the length of the fiber. This cannot be predicted by PBC.

4. RESULTS AND DISCUSSIONS

4.1. Computational results of the first FE model – effect of transverse force application

The aim of the analysis of the first FE model, or essentially, the RVE, was to find the approximate values of force at which the interfacial debonding occurred and, hence, the RVE failed. The calculations from the Newton-Raphson method in ANSYS 12 are highly non-linear and therefore, the values obtained were approximate. Some of the important values of loading are given in Table 3.

Table 3. Selected values of force and their significance.

Force Applied (N)	*Significance*
100000	Well before delamination
445415.2	Approximate force when delamination occurs
9500000	Complete detachment of fiber and matrix

The stress distribution in the direction of the application of force, or loading (i.e. x-direction and the interfacial separation) was investigated in the. It was clearly visible at 100000 N that the RVE was completely intact and that there was no debonding between the fiber and the matrix. The characteristic length of separation for the cohesive zone was also found to be within limits of the exponential CZM. The value for maximum stress in the RVE was noted as 18.746 MPa and can be seen in Figure 19. The maximum stress was observed as being transmitted around the loading region and parallel to it; from the matrix to the fiber through the interface. The maximum stress was concentrated along the x-axis, therefore, throughout the RVE and before debonding, without reaching the mid-portion of the fiber. The minimum stress of 2.124 MPa was observed at the top of the RVE, exactly 90° apart from the region of the maximum stress concentration. This behavior was expected and reaffirmed that the RVE construction was appropriate. The stress values in the matrix followed a pattern of decrease either side of the x-

axis uniformly. This was due to application of PBC. The decrease of stress in the fiber was much slower than that of the matrix indicating its greater stress carrying capacity.

The maximum interfacial separation was found to be 4.2 X 10^{-6} mm which was less than the characteristic interfacial separation at debonding for the exponential CZM at 1.15 X 10^{-5} mm. This was as expected, but verified the fact that the interface came into play when any amount of force was applied to the RVE. The interfacial separation at 100000 N is shown in Figure 20.

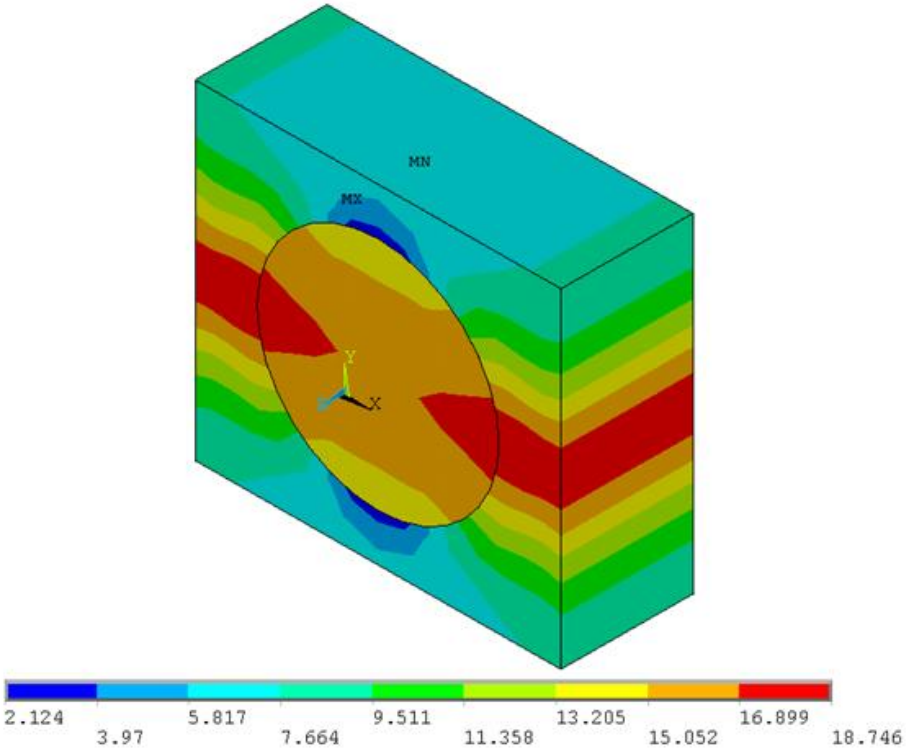

Figure 19. Stress distribution in the x-direction at 100000 N for the RVE.

The debonding phenomenon was found to occur when the force was approximately 445415.2 N. The stress distribution in x-direction, for the RVE, is shown in Figure 21. The maximum stress rose to 239.863 MPa and was concentrated in the matrix. It is important to note that the region where this maximum stress occurred was the region where there had been minimum stress concentration, previously, and the trend of stress distribution all over had reversed with the stress decrease coming from y-axis to the other regions. This was clearly

attributed to the failure of the entire interface due to which the stress did not reach the fiber at all and, hence, the composite lost most of its stress carrying capacity. The reason that the maximum stress region was so formed is that the deformation of the matrix occurred in such a manner that those regions were pulled down upon the interface and fiber. Since the interface had failed already, however, there was no stress transmission to the fiber.

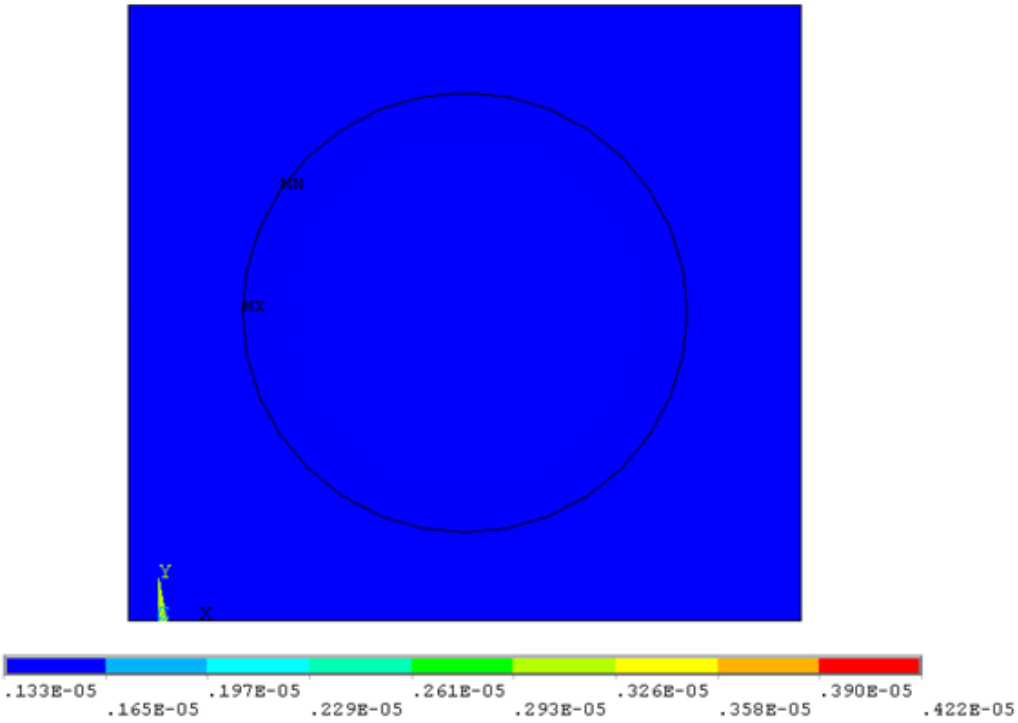

Figure 20. Interfacial separation at 100000 N for the RVE.

The complete failure of the interface can be confirmed from Figure 22 which shows the interfacial separation for the RVE at 445415.2 N. The minimum separation in the interface was 0.293 mm which was over the characteristic interfacial separation. No region of the interface, therefore, joined the fiber and the matrix. This is the reason that there was no stress in the fiber. The maximum separation shown by the red region is 1.962 mm. This was over the characteristic interfacial separation, a great deal, indicating which region failed the earliest. The pattern of separation seen in Figure 22 was again due to the effect of PBC and the stress pattern was,

therefore, correspondingly in opposite tune with the interfacial separation. The pattern set a precedent for how failure proceeded in the interface.

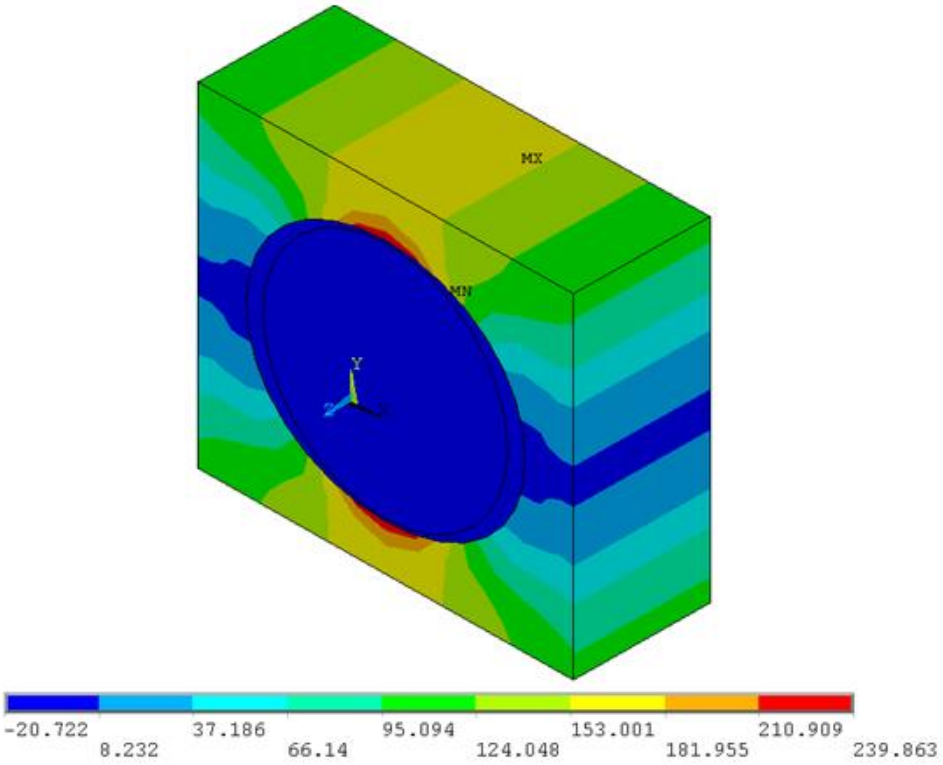

Figure 21. Stress distribution in x-direction at 445415.2 N for the RVE.

The behavior of the RVE at a force of 9500000 N was observed to follow the previous case of, namely – the point of debonding. As expected the stress values were comparably higher and they followed a similar pattern as to when debonding occurred in the RVE. The maximum stress was observed as 5116 MPa and was concentrated in the same regions where the matrix had been pulled into the fiber. Again, the fiber did not carry any stress due to failure of the interface. This can be seen in Figure 23.

The interfacial separation seen in Figure 24 is also similar to when the debonding in the RVE occurs except the values are again considerably higher when compared to the previous case. The pattern seen in Figure 24 is again similar to what is presented in Figure 22. The

minimum separation was 6.25 mm and the maximum separation was 41.843 mm. Both values were much higher than the characteristic interfacial separation.

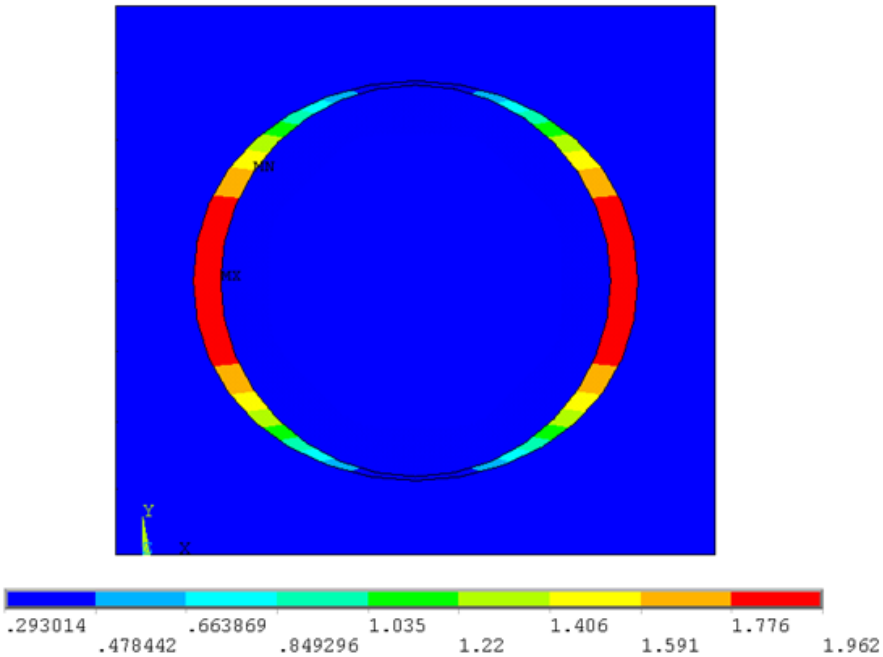

Figure 22. Interfacial separation at 445415.2 N for the RVE.

Two elements within the interface were selected to record the values of the stresses that occurred in the interface at specific locations. These two elements, and the element numbers, can be seen in Figure 19. The significance of the location of these two elements can be interpreted from the fact that the maximum stress concentration occurs near element number 723 before debonding and the least amount of stress occurred after the debonding of an opposite behavior was observed near element number 700. The interfacial stress and interfacial separation for these two elements at the aforementioned important values of force (in Table 3) are recorded in Table 4. The values in Table 4 roughly followed the behavior shown in the curve in Figure 2 (a) for the interfacial stress versus interfacial separation.

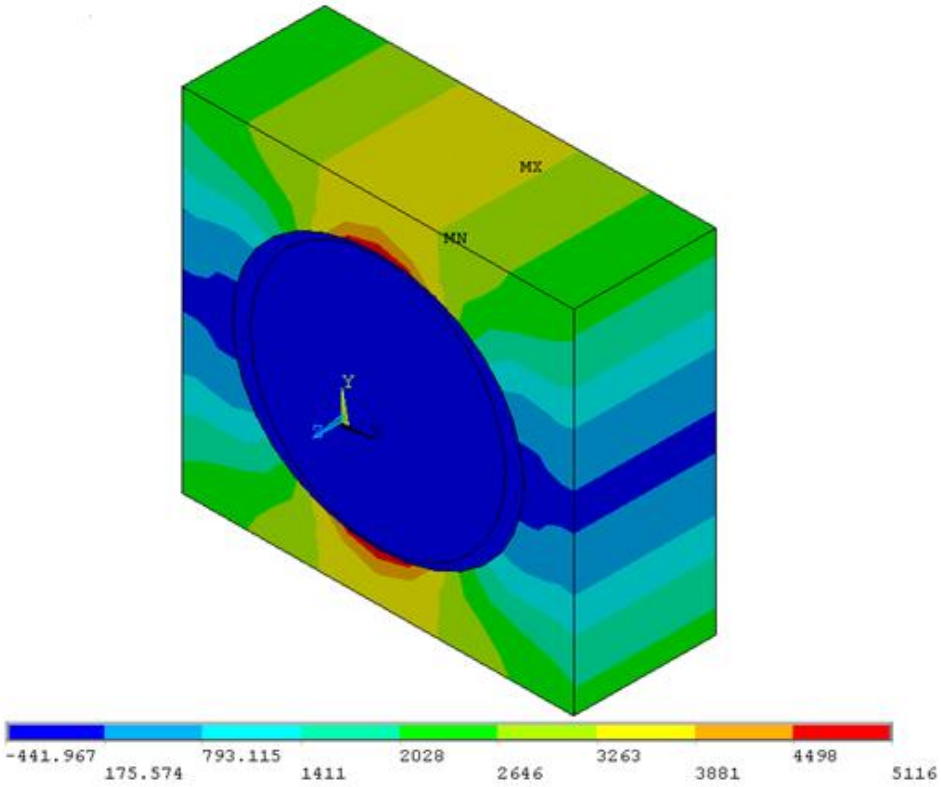

Figure 23. Stress distribution in x-direction at 9500000 N for the RVE.

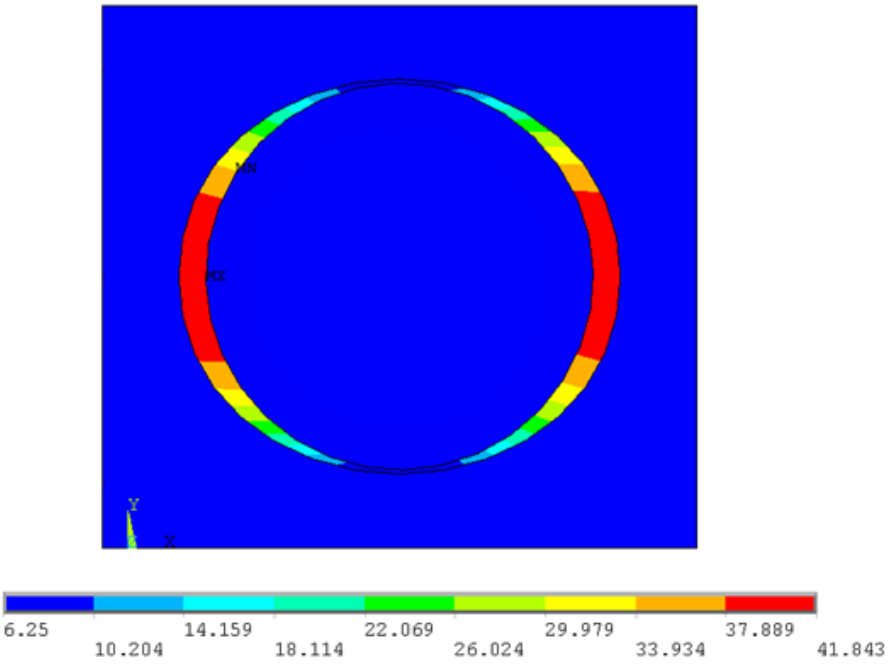

Figure 24. Interfacial separation at 9500000 N for the RVE.

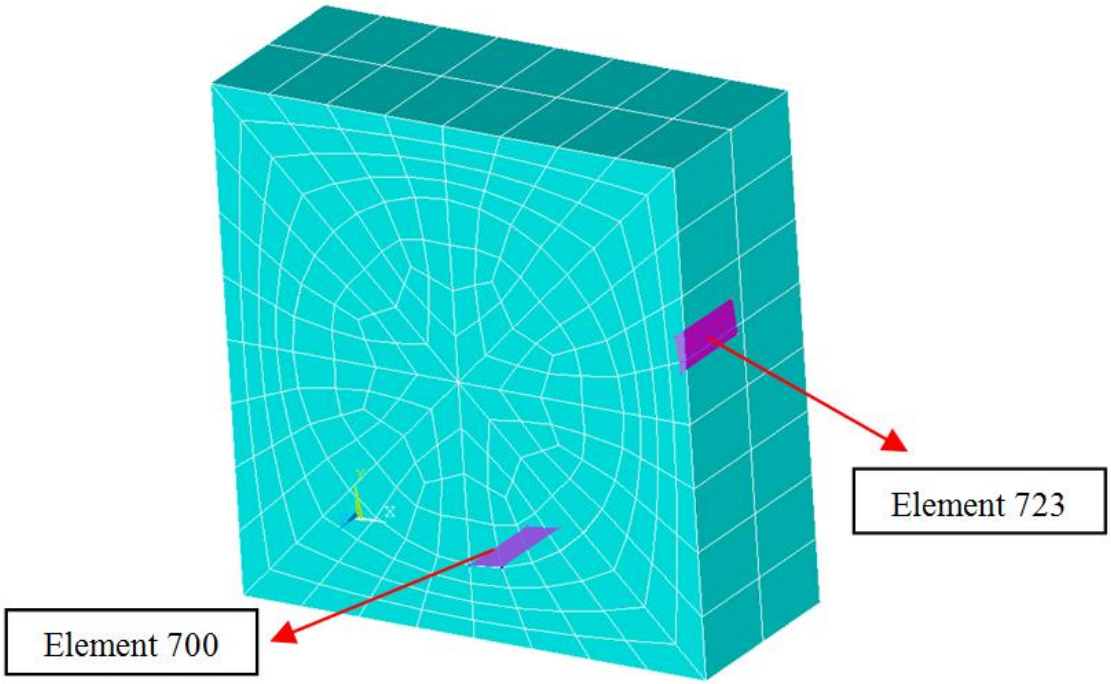

Figure 25. Element numbers 700 and 723 selected to record the interfacial stresses experienced at the point of fiber-matrix debonding.

The stress values were observed to immediately reach zero when the interface failed and there was not further stress transfer from the matrix to the fiber. Both the interfacial elements had maximum stresses below the characteristic stress values of the interface for 100000 N. The maximum stress in element 723 at 445415.2 N was 68.527 and this indicated the structure was very close to failure.

Table 4. Interfacial stress and interfacial separation for elements 700 and 723 at different forces.

Force (N)	100000		445415.2		9500000	
Interfacial Element	700	723	700	723	700	723
Maximum Interfacial Stress (MPa)	4.946	15.368	20.429	68.527	0	0
Minimum Interfacial Stress (MPa)	0.249	0.76	0	0	0	0
Maximum Interfacial Separation (mm)	1.326×10^{-6}	4.22×10^{-6}	0.293	1.962	5.865	41.549
Minimum Interfacial Separation (mm)	6.569×10^{-8}	2.012×10^{-7}	2.93×10^{-7}	9.035×10^{-7}	0.293	2.072

4.2. Experimental

The number of total samples prepared for pull-out tests was 10. The results from two successful specimens were selected since these were the two samples that exhibited a clean fiber pull-out without matrix failure. The holes in the matrix specimens were also seen to have a measurable area and perimeter under the microscope. These specimens were free of any fibers sticking out of the holes in the matrix. The specimens in which fiber failure occurred had an impregnation depth greater than 1.63 mm. This depth was achieved after repeatedly reducing the impregnation depth of the specimens where fiber failure took place. A few other samples underwent matrix cracking and complete matrix failure which required the need to increase the thickness of the matrix.

The pull-out tests demonstrated that the interfacial failure for the E-glass fiber epoxy matrix composite specimens occurred at a certain maximum value of force, and this was in a consistent region. This can be seen in the force-displacement curves in Figure 27 (a) and (b) obtained from the experimental results of the pull-out tests. For successful specimens, the pull-out force (F_{max}) was observed to be as follows:

1. Specimen 1: 58.07 N
2. Specimen 2: 56.91 N

When there is complete debonding or interfacial failure in the composite this force is reduced instantly by a huge value. The area under the force-displacement curve up until this point is, therefore, the energy stored in the interface and required to overcome in order for the interface to fail. This stored energy (G_{ct}) is released when interfacial failure occurs and this is the reason that the force is suddenly reduced to a low value. The area under the curve is the raw experimental data from the pull-out tests and is calculated by a MATLAB® (Mathworks Inc.)

program which gives an accurate measure of the energy. This program is given in the section Appendix. Area Under The Force-Displacement Curve.

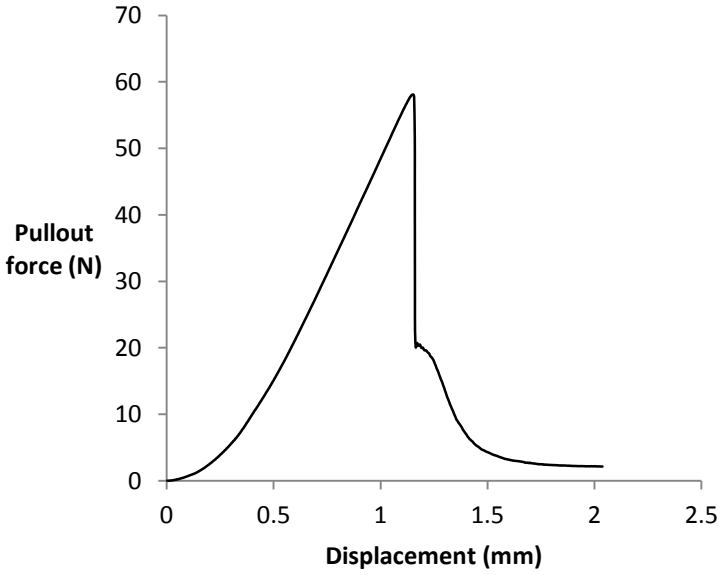

(a)

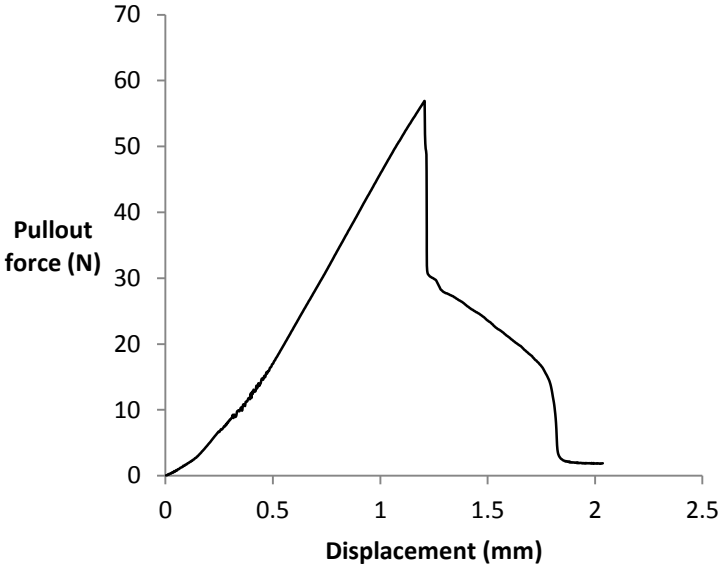

(b)

Figure 26. Force-Displacement curves obtained from the pull-out tests where drastic fall in force was observed at failure (interfacial debonding): (a) Specimen 1 – Pull-out force: 58.074 N, (b) Specimen 2 – Pull-out force: 56.917 N

The value of the force in the force-displacement curve does not reach zero immediately after the fiber-matrix debonding, but there is some residual energy due to the fiber being embedded in the rubber gasket. The behavior of the curve in Figure 26 (a) and (b) after interfacial failure can, therefore, be attributed to the frictional force required to pull the fiber bundle out of the rubber gasket.

The two parameters of the bilinear cohesive zone – characteristic interfacial shear strength (τ_{max}) and characteristic interfacial shear separation (δ_{max}), are obtained from the average of the two experimental values shown in Table 5. The data derived from the pull-out test can be directly applied in the FE study by modeling of the CZM since the properties of the CZM are dependent on the two main parameters - τ_{max} and δ_{max}. τ_{max} is calculated from equation 19 where F_{max} is the maximum pull-out load (Page 62) obtained from the experimental tests. δ_{max} is obtained from equation 18 – G_{ct} is calculated from the experiment; area under the curve from Figure 26 (a) and (b) as explained earlier; while τ_{max} is calculated from equation 19 previously. Thus the values shown in Table 5 are a direct interpretation of the experimental data and implemented into the FE study as properties of a bilinear CZM.

Table 5. The values of characteristic interfacial shear strength and characteristic interfacial shear separation obtained from pull-out tests.

Specimen Number	τ_{max} *– Characteristic interfacial shear strength (MPa)*	δ_{max} *– Characteristic interfacial shear separation (mm)*
1	13.148	4.029
2	13.550	4.403
Average	13.349	4.216

4.3. Computational results of the second FE model – variation of δ_{max}

A parametric study of δ_{max} is performed keeping τ_{max} constant at the experimental average value of 13.349 MPa from Table 5. This study was aimed at observing the effect of changing the

characteristic length of the interface and the corresponding shear stresses as experienced by the composite during pull-out. The values of δ_{max} considered for this study were as follows:

1. 1.054 mm – 1/4th of experimental average;
2. 2.108 mm – 1/2 of experimental average;
3. 4.216 mm – experimental average; and
4. 8.432 mm – twice of experimental average.

The debonding (referred to as 'failure' from here on in) of the interface for the first value of δ_{max} occurs at a pull-out load of 27.7 MPa. This is the weakest interface. The interfacial shear stress distribution and the stress distribution in the principal direction of the composite structure for all values of δ_{max} is, therefore, compared at, or before, a pull-out load of 27.6 MPa.

Pull-out loading is applied to the composite structure after constraining it as mentioned in section 3.4. The applied loading appropriately simulates the pull-out force from the experimental tests since the pressure transmits the force on the fiber bundle in a uniform manner which is then transmitted through the interface to the matrix. The role of the interface can be studied, therefore, in a comprehensive manner by observing the interfacial shear stress distribution patterns. This shear stress pattern has an effect on the overall strength of the composite structure which is further studied to determine the change in behavior of the structure. The interfacial shear stress distribution patterns, for all four values of δ_{max} mentioned earlier, are observed to be similar in a consistent manner until a pull-out loading of 22 MPa. This is demonstrated in Figure 27 (a), (b), (c) and (d). As δ_{max} is increased in the order of the four aforementioned values, the strength of the interface keeps increasing slightly. This increase in the strength of the interface, however, did not affect the overall strength of the composite structure. This can be inferred from the normal stresses developed in the structure which had negligible effect for 22 MPa loading. The

interfacial stresses reach a maximum of 13.349 MPa since this is the characteristic strength of the interface.

When the loading reaches 25 MPa, the interfacial stresses followed a distribution pattern as seen in Figure 28 (a), (b), (c) and (d). The stress distribution pattern for δ_{max} = 1.054 mm in Figure 28 (a) shows that stress relaxation started to occur in the direction of the application of the pull-out load. The region of the maximum shear stress which performed most of the load transfer from the fiber to the matrix, was observed to be defined to a particular area. This region shifted in the direction opposite of the pull-out load application. All the other interfacial shear stress patterns for different values of δ_{max} seen in Figure 29 (b), (c) and (d) showed no relaxation, but the region of maximum stress carrying capacity kept increasing.

A further increase of the pull-out load to 27.6 MPa showed that for δ_{max} = 1.054 mm seen in Figure 29 (a), underwent further stress relaxation. The region of maximum shear stress shifted backwards more as compared to when the loading was 25 MPa. For δ_{max} = 2.108 mm, the same loading of 27.6 MPa incurred a stress relaxation in the interfacial shear stress distribution pattern. This can be seen in Figure 29 (b).

The other two interfaces, for the two values of δ_{max}, showed an increase in the region of the maximum shear stress as seen in Figure 29 (c) and (d). It can be inferred from these observations that the region of maximum shear stress in the interface was responsible for transferring the shear stress from the fiber to the matrix.

When the value of δ_{max} was reduced, it was observed that for a weaker interface, when the loading values were close to failure, the region of maximum shear stress was smaller. This was verified by the stress relaxation observed in the interface when δ_{max} = 4.216 mm

(experimental average) at a pull-out load of 28.9 MPa as seen in Figure 30. This was the load just before failure of the interface for δ_{max} = 4.216 mm.

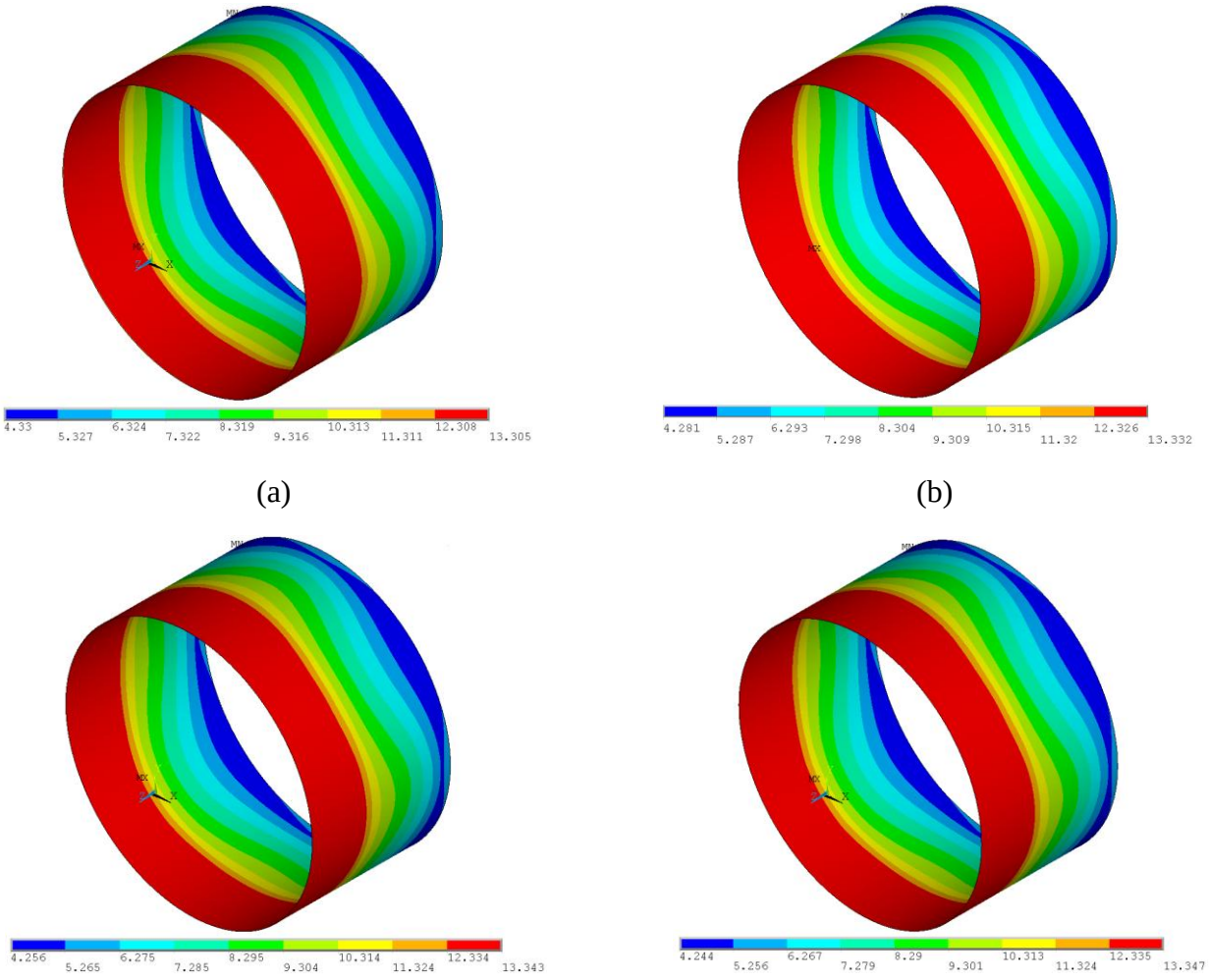

Figure 27. Interfacial shear stress distribution at 22 MPa pullout loading for: (a) δ_{max} = 1.054 mm, (b) δ_{max} = 2.108 mm, (c) δ_{max} = 4.216 mm, (d) δ_{max} = 8.432 mm

Based on observation of the stress relaxation phenomenon, it can be concluded that the maximum shear stress region in Figure 30 was visibly larger than the region of the other two weaker interfaces (lesser values of δ_{max}) before each of the interfaces failed. The maximum shear stress carrying capacity for a particular interface before failure was dependent on δ_{max}.

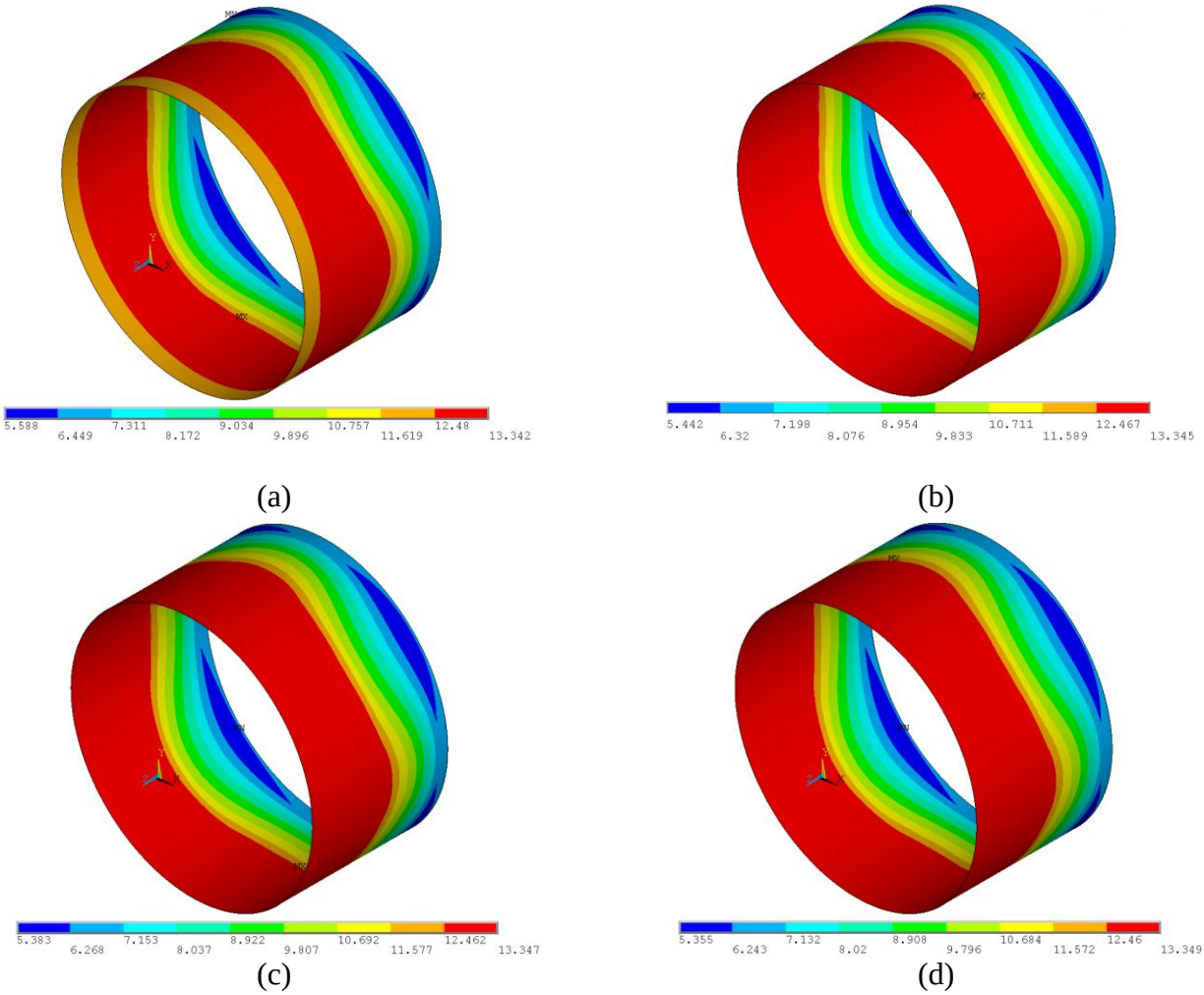

Figure 28. Interfacial shear stress distribution at 25 MPa pullout loading for: (a) δ_{max} = 1.054 mm, (b) δ_{max} = 2.108 mm, (c) δ_{max} = 4.216 mm, (d) δ_{max} = 8.432 mm

The reason for this occurrence can be attributed to the change in shape of the traction-separation curve investigated by Chandra et al. [15]. Their study confirmed that changing the δ_{max} changed the shape of the traction-separation curve and, thus, the shape of the curve influenced the region of the maximum shear stress of the interface.

The increase in the value of δ_{max} increased the maximum compressive stress generated in the matrix as the pull-out load was increased on the fiber. It was observed that these maximum compressive stresses are developed in the matrix in a region nearest to the interface. The maximum compressive stresses for δ_{max} = 1.054 mm and δ_{max} = 16.864 mm were particularly

observed for the study. For a pull-out load of 10 MPa, the compressive stresses remained almost the same as seen in Figure 31 (a) and (b).

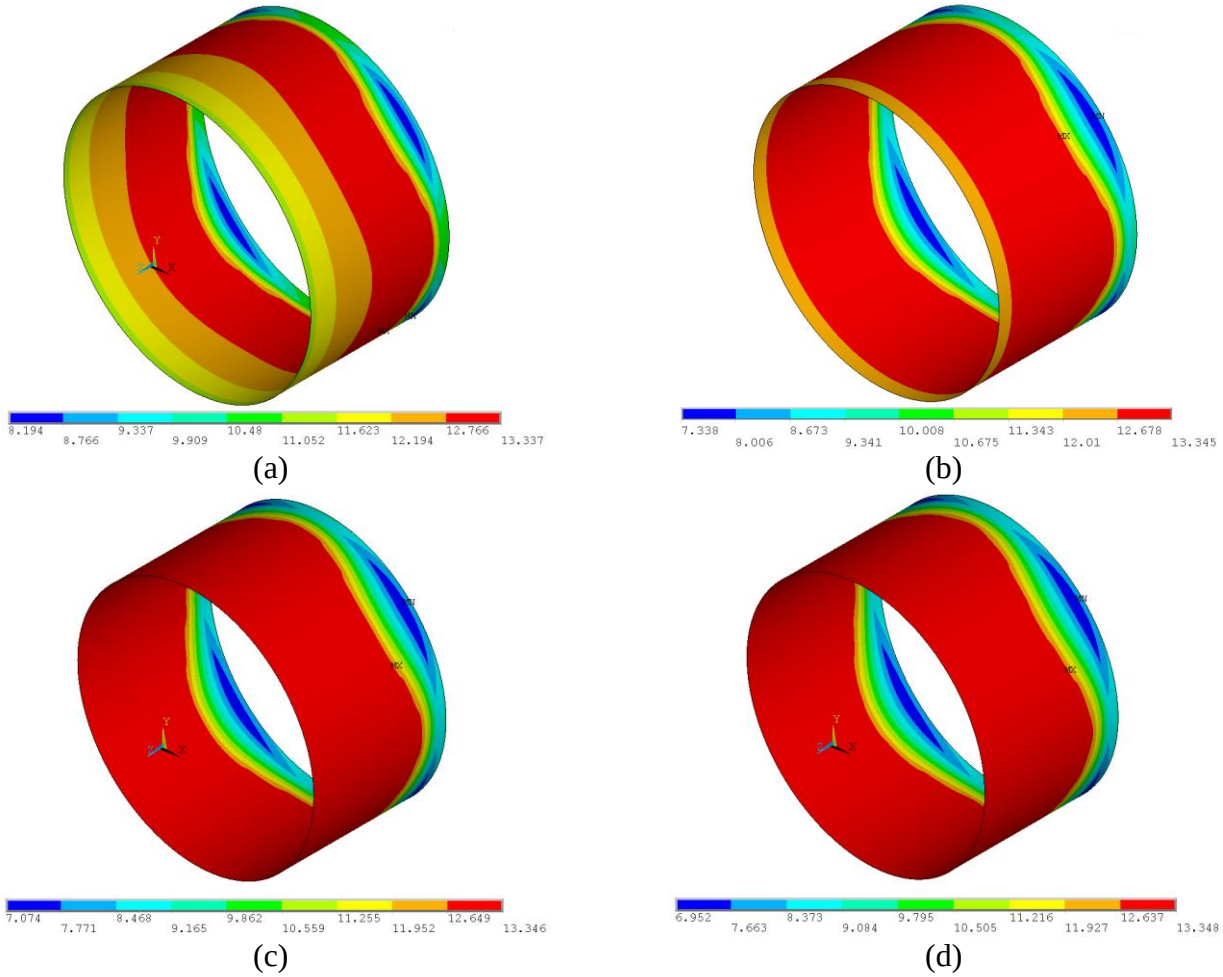

Figure 29. Interfacial shear stress distribution at 27.6 MPa pullout loading for: (a) δ_{max} = 1.054 mm, (b) δ_{max} = 2.108 mm, (c) δ_{max} = 4.216 mm, (d) δ_{max} = 8.432 mm

When the pull-out load was increased to 27.6 MPa, these stresses rose from 48.532 MPa for δ_{max} = 1.054 mm to 52.401 MPa for δ_{max} = 16.864 mm as seen in Figure 31 (c) and (d). This phenomenon can, therefore, be attributed to the higher bond strength and to the greater resistance to failure for a stronger interface. This bonding strength was a direct consequence of the region of maximum shear stress, wherein, – larger the area of the maximum shear stress, the comparatively better bonding.

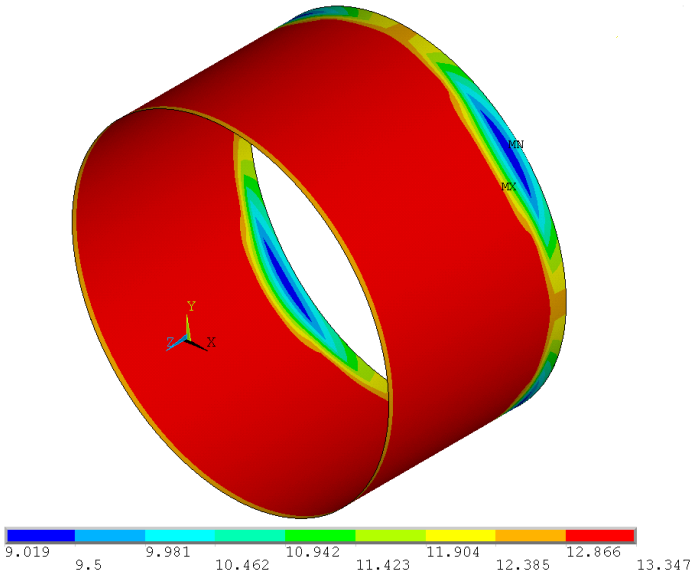

Figure 30. Interfacial shear stress distribution at 28.9 MPa pull-out loading for δ_{max} = 4.216 mm (experimental average) – stress relaxation is seen to occur just before failure.

The pull-out force, or traction, values at failure, for different values of δ_{max}, for the composite structure are provided in Table 6. These values explain how the interface failed according to the shear traction and why the composite structure experienced the relative differences in its strength with variance in δ_{max}.

The values in Table 6 show that for the first increase of 1.054 mm in δ_{max}, the force required to fail the composite increased by 3198 N. For a subsequent increase of 2.108 mm to 4.216 mm in δ_{max}, the force increased by 1999 N. When the value of δ_{max} rose to 8.432 mm, the force required for failure increased by 1599 N. For the final increase of δ_{max} to 16.864 mm, the force increased by 799 N. There was, therefore, a decrease in the force with an increase in δ_{max}.

The variation of δ_{max} against traction for the composite structure at failure is given by the curve in Figure 32. A logarithmic relationship between the two was found which can be represented by the following equation:

$$P_L = 2.712ln(\delta_{max}) + 111.39 \quad (27)$$

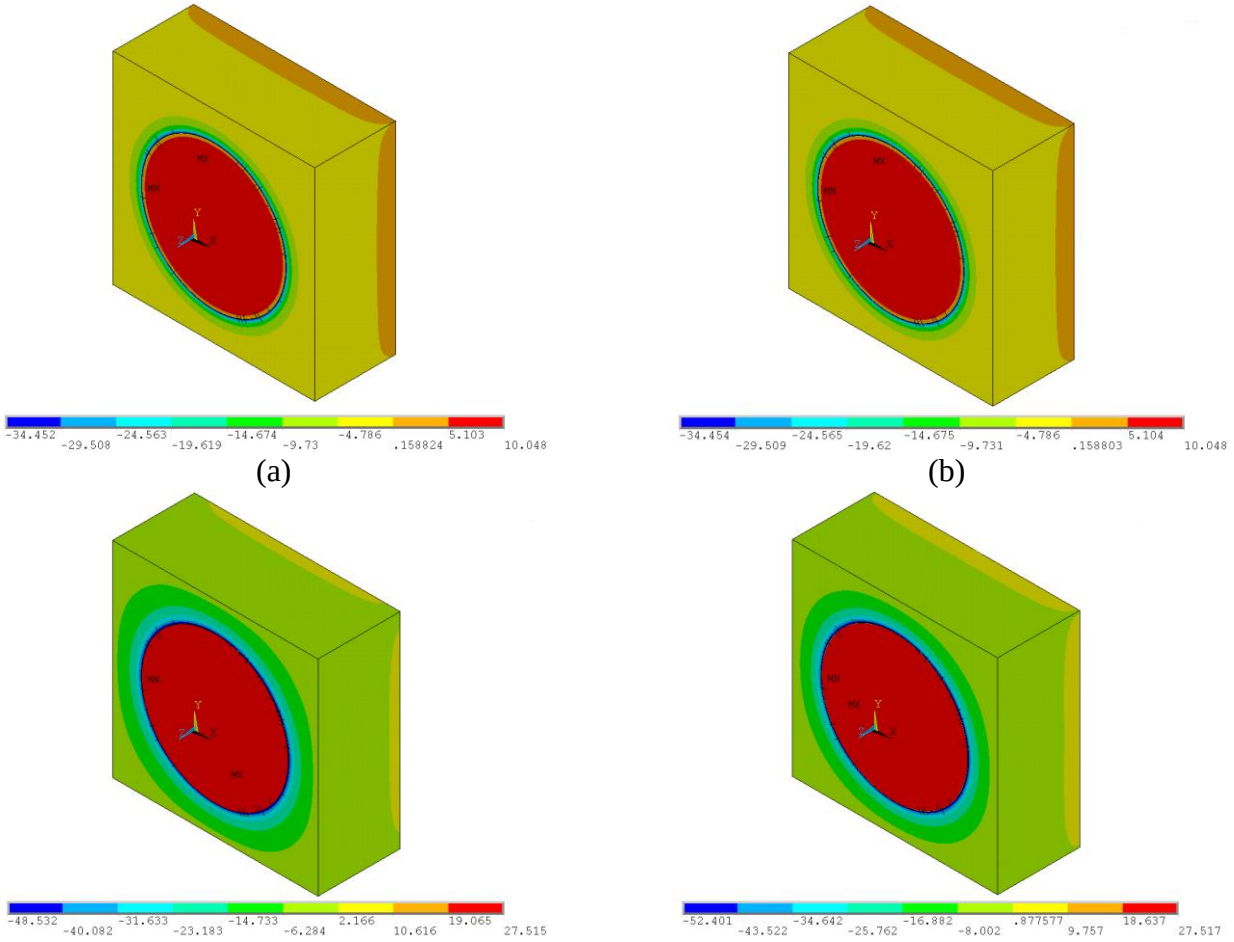

Figure 31. Normal stress distribution in the direction of application of force for the composite structure at: (a) pullout loading 10 MPa for δ_{max} = 1.054 mm, (b) pullout loading 10 MPa for δ_{max} = 16.864 mm, (c) pullout loading 27.6 MPa for δ_{max} = 1.054 mm, (d) pullout loading 27.6 MPa for δ_{max} = 16.864 mm

P_L in equation 27 represents the pull-out loading. Equation 27 has a coefficient of determination of 0.947. Therefore pull-out loading values predicted by the relationship can be assumed to be fairly close to the behavior exhibited by the FE model. The relationship clearly indicates that the strength of the composite, with respect to interfacial failure, decreased at a much higher rate as the value of δ_{max} decreased below the experimental average value. Increasing the value of δ_{max} above the experimental average increased the strength of the composite, but at a

markedly slow rate. This was again, because of the shape of the traction-separation curve was altered with varying values of δ_{max}.

Table 6. Pull-out force (traction) at failure for the composite structure for different values of δ_{max}:

δ_{max} *(mm)*	*Pull-out force (kN)*
1.054	110.728
2.108	113.926
4.216	115.925
8.432	117.524
16.864	118.323

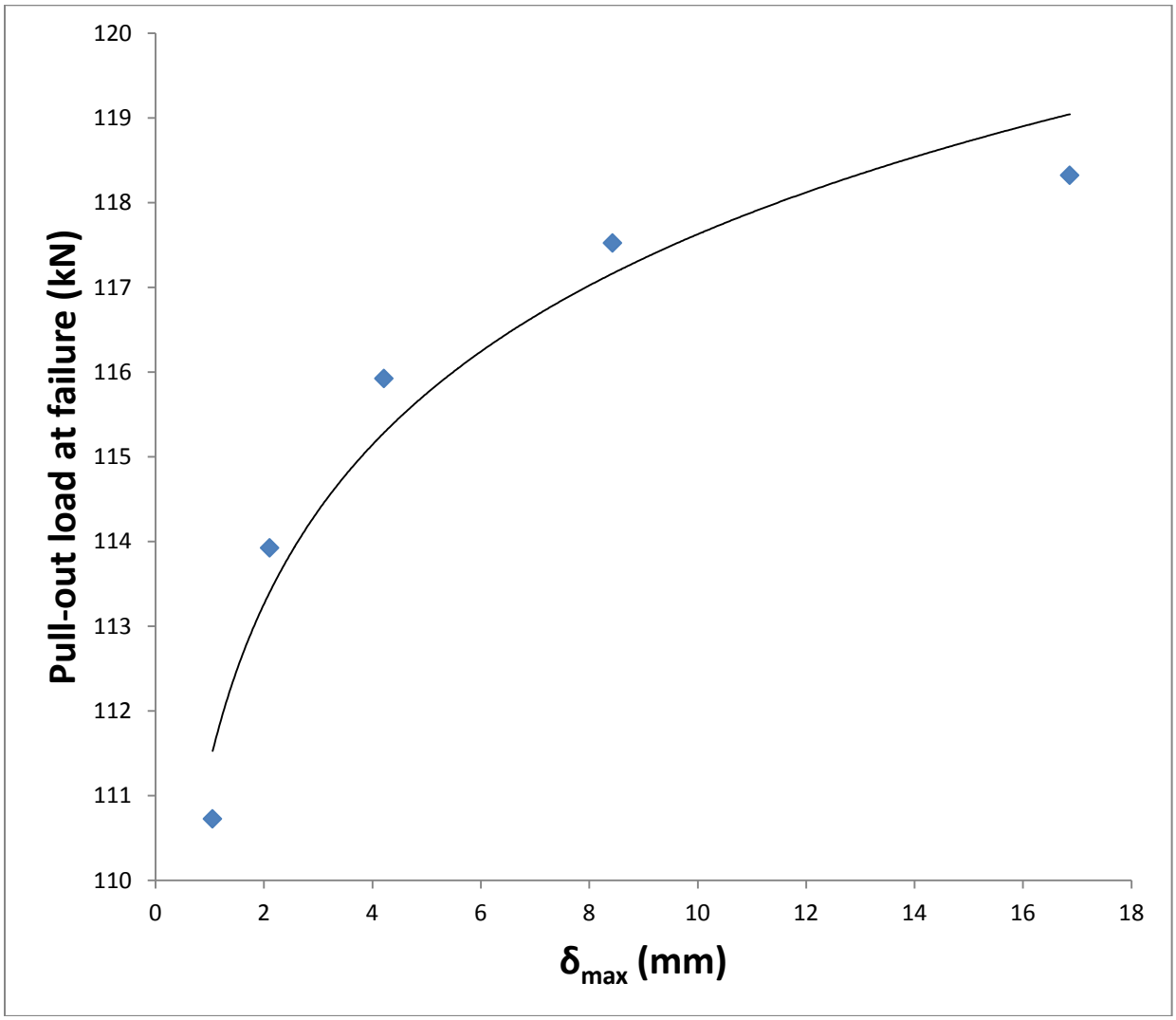

Figure 32. Variation of δ_{max} on pull-out load (traction) for the composite structure at failure.

4.4. Computational results of the second FE model – variation of δ_{max}

A similar parametric study to that of variation of δ_{max} was performed for the variation of τ_{max}. This was done by keeping the δ_{max} constant at the experimental average of 4.216 mm. In general, the variation of τ_{max} had a greater impact on the interfacial shear stress pattern than the variation of δ_{max}. It was necessary, therefore, for the two values of τ_{max} to be in close vicinity to the experimental average to clearly show the visible effect on the stress pattern. The values selected for the parametric study were:

1. 5 MPa – comparatively lesser than experimental average;
2. 10 MPa – less than experimental average;
3. 13.349 MPa – experimental average; and
4. 15 MPa – above experimental average.

As expected, the first interface was the weakest and failed at a pull-out load of 11.1 MPa. When comparing all four of the interfaces, therefore, they must be compared at, or below 11 MPa. A pull-out load of 8 MPa was applied to composite structure. The shear stress distribution pattern for τ_{max} = 5 MPa is shown in Figure 33.(a). This is visibly different than the shear stress distribution pattern for τ_{max} = 10 MPa, 13.349 MPa and 15 MPa shown in Figure 33 (b), (c) and (d) respectively, and with the regions of various values of shear stress varying quite distinctively. This behavior in the interface (i.e. distinctive variation of shear stress patterns) was not observed in case of variation of δ_{max} even when there was a high increase in its value unless the loading was close to failure. There was no noticeable stress relaxation in the interface for any of the values of τ_{max}. This can be explained from the fact that since δ_{max} does not change, the energy required for failure keeps increasing because the area under the traction-separation curve keeps increasing.

The pull-out loads at failure for the composite structure are given in Table 7. These failure values can also be attributed to the aforementioned fact that the shape of the traction-separation curve corresponds to the values of δ_{max}.

It can also be seen in Figure 34 (a), (b), (c) and (d) that for a loading of 8 MPa, a stronger interface (with respect to variation of τ_{max}) has a higher generation of compressive stresses in the matrix. This means that the stress transfer is better for a stronger interface. This trend was followed as the loading was increased.

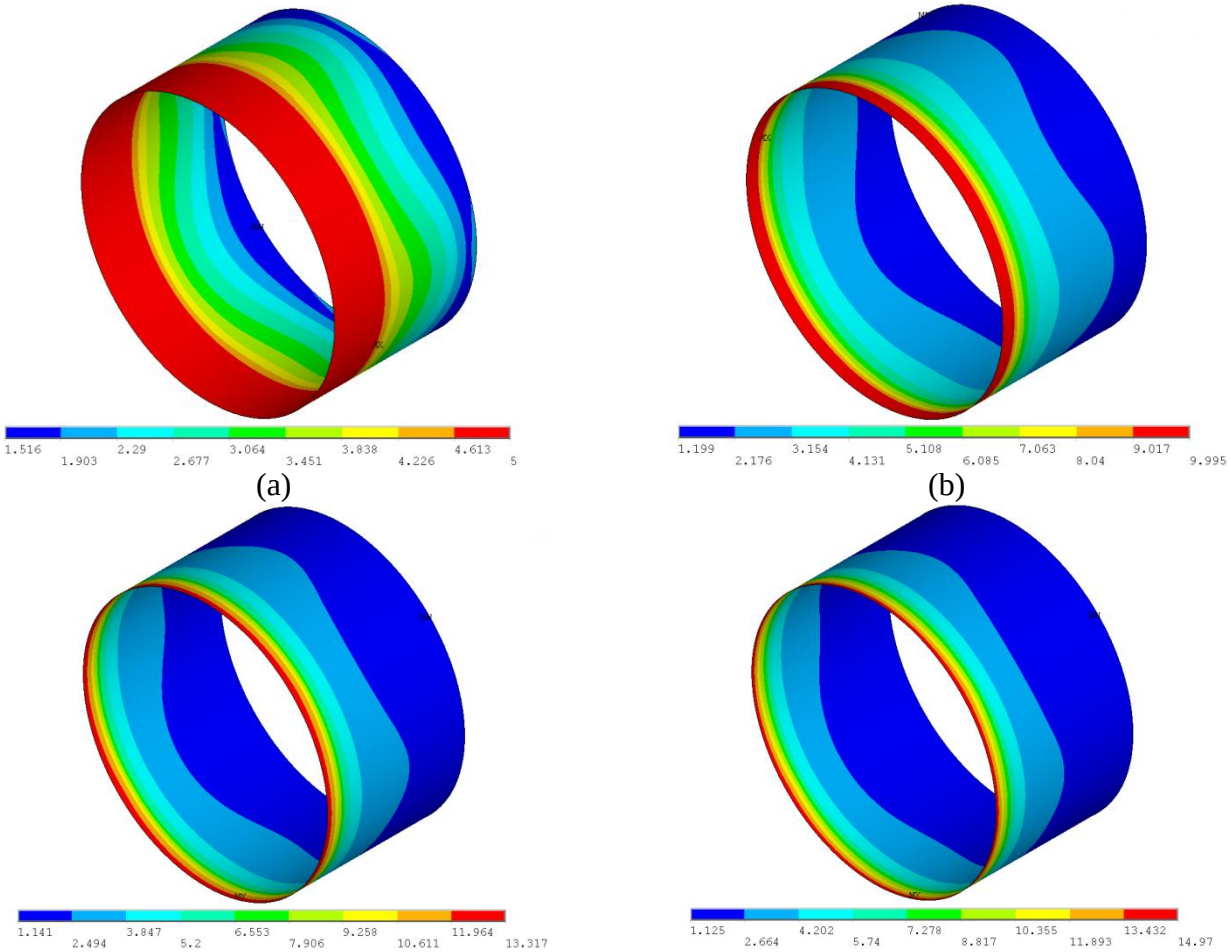

Figure 33. Interfacial shear stress distribution at 8 MPa pullout loading for: (a) τ_{max} = 5 MPa, (b) τ_{max} = 10 MPa, (c) τ_{max} = 13.349 MPa, (d) τ_{max} = 15 MPa

Table 7. Pull-out force (traction) at failure for the composite structure for different values of τ_{max}:

τ_{max} *(MPa)*	*Pull-out force (kN)*
5	44.371
10	87.143
13.349	115.925
15	130.715
20	172.688

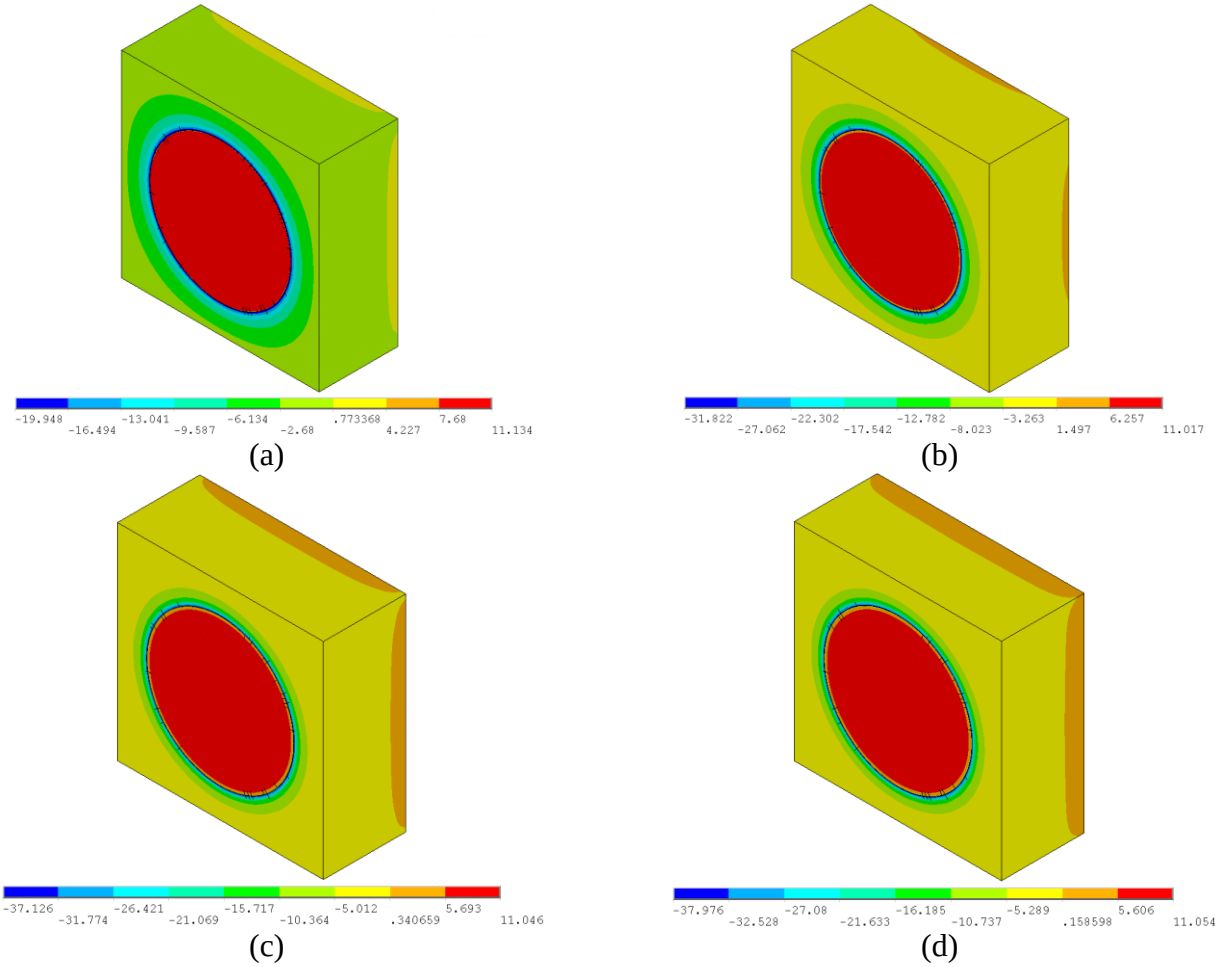

Figure 34. Normal stress distribution in the direction of application of force in the composite structure at 8 MPa pullout loading for: (a) τ_{max} = 5 MPa, (b) τ_{max} = 10 MPa, (c) τ_{max} = 13.349 MPa, (d) τ_{max} = 15 MPa

The overall composite structure gained significant strength with increase in τ_{max} from the observation of stress distribution in the composite structure in its loading direction. The transfer of stress also improved with a stronger interface. This is because the relationship between the

characteristic strength of the interface and the pull-out loading is linear as shown in Figure 35. The pullout loading values at failure, in Table 7 support this, as well. The shape of the traction-separation curve played a vital role in these findings as explained earlier. Equation 28 gives the relationship between pull-out loading and characteristic shear strength of the interface.

$$P_L = 8.57\tau_{max} + 1.5879 \quad (28)$$

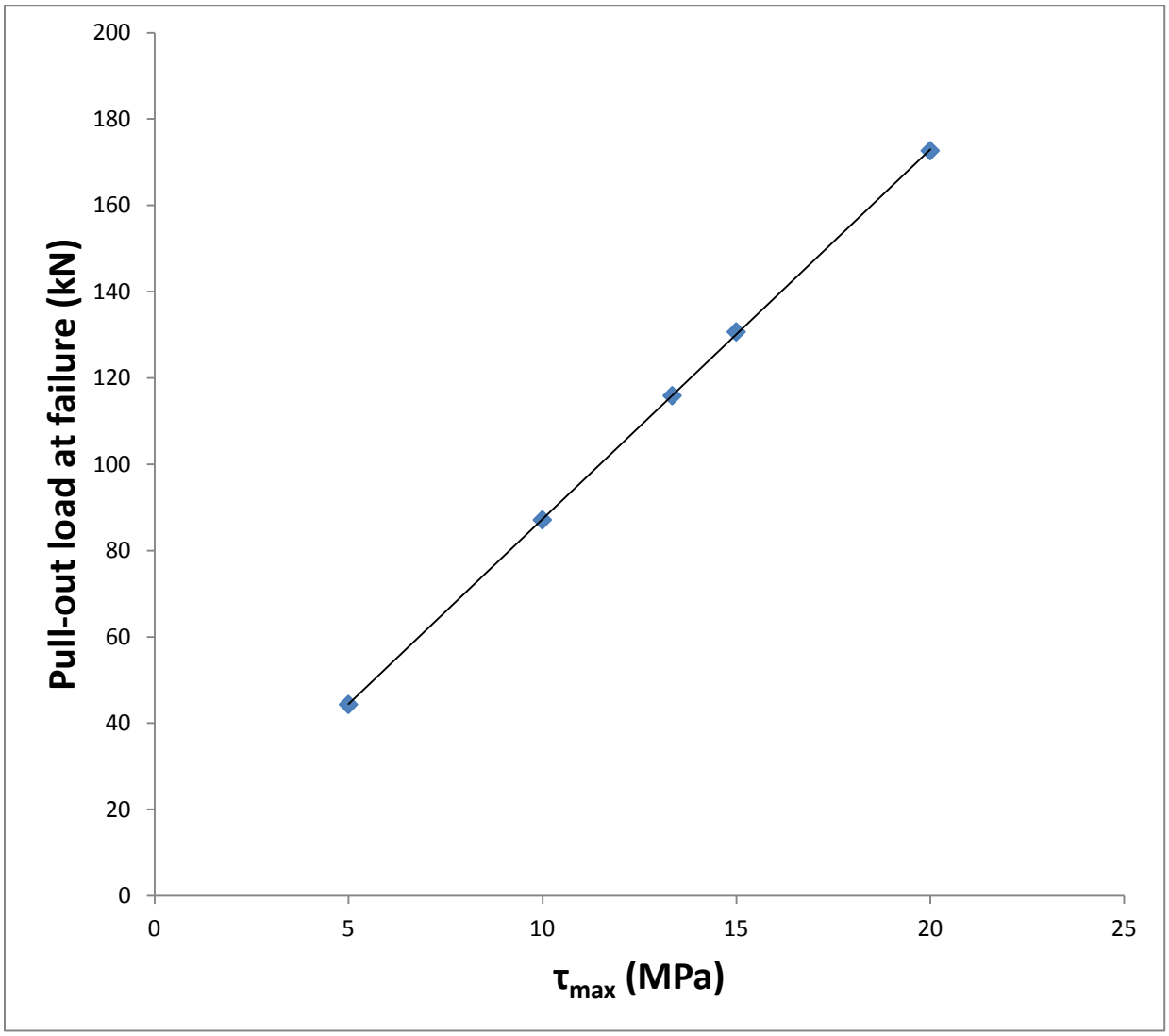

Figure 35. Variation of τ_{max} on pull-out load (traction) for the composite structure at failure.

4.5. Validity of results

The first FE model showed behavior consistent with the exponential CZM relationship followed in equation 5 and seen in Figure 2.(a). The aim of the first FE model was to show that the fiber-matrix interface could be used in further studies in the form of individual elements constructed together to form a consistent entity which would behave independently of both the fiber and the matrix. The non-existence of stress transfer from the matrix to the fiber seen in Figure 21 and 23 after interfacial failure ascertains that the interface construction was appropriate for a transverse load application.

In the second FE model, the stress transfer phenomenon in the interface can be justified based on the behavior of the interface. The behavior of the interface seen when both δ_{max} and τ_{max} are varied is consistent in accordance with the bilinear CZM relationship followed equation 18 and seen in Figure 5. This is only possible if the interface has reached its maximum potential. The properties of the interface in the FE study have been obtained from the pull-out testing done on glass fiber epoxy matrix composites. The relationship between pull-out testing and FE modeling has been explained in section 3.4.

Figure 27 (a), 28 (a), (b) and 29 is indicative that stress relaxation takes place in the interface; therefore stress relaxation is a feature observed when δ_{max} is varied. No stress relaxation takes place in Figure 33 (a), (b), (c) and (d); therefore stress relaxation is not a feature when τ_{max} is varied. This is verified from:

1. Figure 32 and equation 27 – logarithmic relationship between pull-out loading and δ_{max}.
2. Figure 35 and equation 28 – linear relationship between pull-out loading and τ_{max}.

The difference in the relationships when δ_{max} and τ_{max} are varied respectively tells us that the each is independent of the other when influencing the pull-out load. If both the relationships

had shown the same pattern i.e. both logarithmic or both linear then we would have ascertained that there would not have been any need to keep one of them constant and vary the other.

To show the validity of the FE modeling and the CZM structure, an interface with the following properties was considered [32]:

τ_{max} = 39 MPa

φ = 18.075 N/mm

δ_{max} = 0.927 mm

This represents an increase in strength of the interface in terms of τ_{max} but δ_{max} is reduced to show that the region of maximum shear stress transfer is dependent on δ_{max}. The composite structure is subjected to a pull-out loading of 62 MPa to clearly show the region of maximum shear stress region and also further relaxation in the interface in Figure 36. The interface undergoes stress relaxation from 38.543 MPa to 35.689 MPa immediately where the region of maximum shear stress region ends. The region of maximum shear stress is dependent on δ_{max} as inferred earlier. There is further stress relaxation in the interface as well, seen in Figure 36 with shear stress bands of 32.835 MPa, 29.981 MPa and 27.128 MPa.

To validate the inference, the composite structure is subjected to a further loading of 68 MPa shown in Figure 37. The region of maximum shear stress is seen to be consistent but retreats backwards in the interface to allow for further stress relaxation to 26.183 MPa. The interface has a higher value of τ_{max} and therefore undergoes stress relaxation rather than complete failure. Comparing the behavior of the maximum shear stress region shown in Figure 36 and Figure 37, it is evident that this area is consistent for the same value of δ_{max} and hence shear stress transfer phenomenon depends directly on δ_{max} while absolute failure of the interface is directly dependent on τ_{max}.

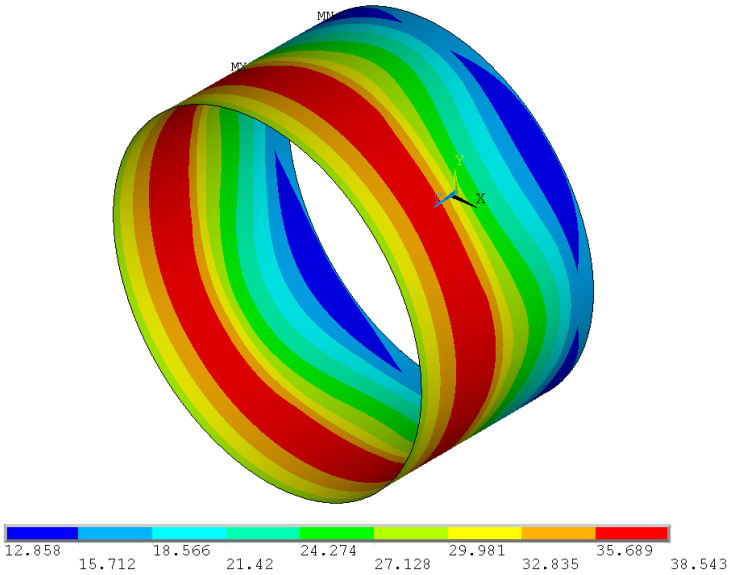

Figure 36. Interfacial shear stress at 62 MPa for CZM with τ_{max} = 39 MPa; δ_{max} = 0.927 mm.

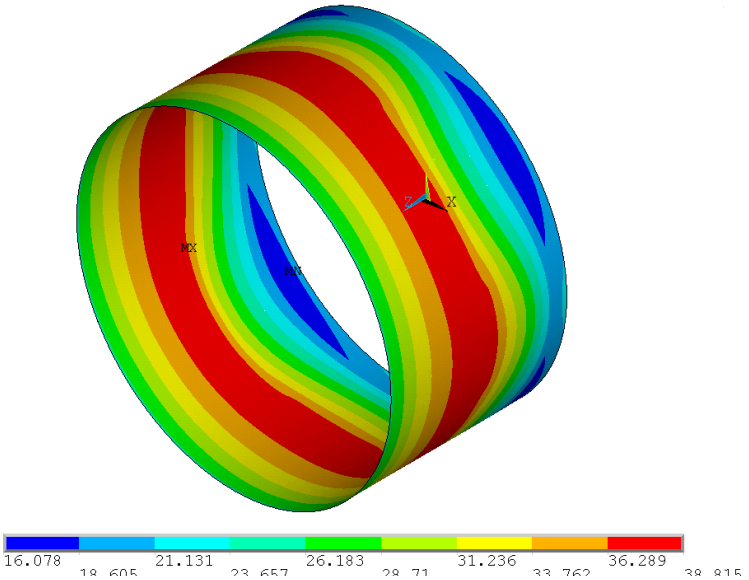

Figure 37. Interfacial shear stress at 68 MPa for CZM with τ_{max} = 39 MPa; δ_{max} = 0.927 mm.

5. CONCLUSIONS

The first FE model was built on the basis that there was no study found in the literature that combined a composite RVE with an interface modeled as a CZM and constrained with PBC. An exponential CZM was incorporated into the composite to model the interface between the fiber and the matrix. The results of the analysis indicated that this model approximately predicted the normal interfacial stresses and the normal stress transfer between the fiber and the matrix in the direction of application of force. This primary model showed that a CZM can determine the behavior of the interface and the subsequent composite RVE after debonding. The stress relaxation caused in the fiber after interfacial failure demonstrated that the interface had a significant effect on the composite due to the loss of stress transfer from the fiber to the matrix compared to the omission of the interface in the study of such a composite. The high strength of the composite can be attributed to the stress carrying capacity of the fiber which was lost when interfacial failure occurred. The FE results indicated that the interfacial separation increased rate in the loading direction. Debonding of the composite leads to matrix fracture since all the stress concentration then occurs in the matrix.

The second FE model for this study was based on the first model, but had a much finer mesh. This was necessary for better prediction of the shear stresses in the interface. The approach of incorporating experimental data obtained from pull-out tests into the computational model of the composite structure, with the help of a bilinear CZM, to predict the response of the interface, was adopted. The interface for the second model of the composite structure at 40% fiber volume ratio, had a characteristic strength of 13.349 MPa and a characteristic separation of 4.216 mm. The shear strength of the interface in model presented here was characterized by the region of the maximum shear stress it could carry before stress relaxation began. This region was

responsible for the maximum stress transfer from the fiber to the matrix. It was observed that this region was dependent upon the value of δ_{max}. This was evident from the observation that increasing the value of δ_{max} did not increase the strength of the interface. This was also indicated by the pullout loading values at failure of the composite structure in Table 6. A logarithmic relationship was found between the two which had a coefficient of determination of 0.947. This means that the pull-out loading predicted by the relationship would closely correspond to the respective δ_{max} and therefore would eliminate the need to experimentally find the pull-out loading at failure. The region of maximum shear stress in the interface was seen to be comparably much larger in area for the experimental average before failure to the other cases and this was the reason that increase in δ_{max} did not affect the value of failure loading significantly even when δ_{max} was increased four times its value.

The overall composite structure gained significant strength with the increase in τ_{max} from the observation of stress distribution in the composite structure in its loading direction. The transfer of stress was also better for a stronger interface. The pullout loading values at failure in Table 7 also supported this since the relationship between the two is a linear one. No stress relaxation in the interface for variation of τ_{max} led further to the belief that the region of maximum shear stress is dependent upon δ_{max} and is unaffected by τ_{max}. The shape of the traction-separation curve played a vital role in these findings, as explained earlier.

6. FUTURE WORK

The model developed in this study considers the unidirectional arrangement of the fibers within the matrix. Fibers within composites are not always oriented unidirectionally. The scope of the study in future can include analyzing the effect of different fiber arrangements like bidirectional, hexagonal or random on the interfacial characteristics of fibrous composites. The results of the pull-out test are used in a bilinear CZM. This CZM can be utilized wherever Mode 2 debonding exists. Bi-directional and hexagonal arrangement of the fibers will cause the arrangement of the fibers within the unit cell to be different compared to the current arrangement. FEM studies investigating pull-out loading on bi-directional and hexagonal undergoing Mode 2 debonding would be the next step in this direction. The variation in arrangement of the fibers would be expected to affect the interfacial stress transfer between the fiber and the matrix in such a way that the overall composite could undergo failure in different ways. The current FE model can be used in future studies as a base model to construct bi-directional or hexagonal models and thus a more complicated overall composite model. Those models could then be used to predict the interfacial shear stress transfer through Mode 2 debonding and the overall stress transfer in the composite corresponding to the current model. The interfacial shear stress transfer from the fiber to the matrix in the future models would behave in the same way as the current model.

In this study both the E-glass fiber and epoxy matrix is considered to be linear elastic and isotropic in nature. Further complexities in terms of material selection for both the fiber and the matrix can be introduced in future studies. Moreover the interfacial characteristics of different fiber and matrix can also be studied using the existing model for various composite applications.

7. REFERENCES

[1] Moon CK. Study on the interfacial properties of three-dimensionally arranged glass fiber/epoxy resin model composites. Journal of Applied Polymer Science 2010;116;1483-1490

[2] Keusch S, Queck H, Gliesche K. Influence of glass fiber/epoxy resin interface on static mechanical properties of unidirectional composites and on fatigue performance of cross-ply composites. Composites Part A 1998;29;701-705.

[3] Thio YS, Argon AS, Cohen RE. Role of interfacial adhesion strength on toughening polypropylene with rigid particles. Polymer 2004;45;3139-47.

[4] Yeung P, Broutman LJ. The effect of glass-resin interface strength on the impact strength of fiber reinforced plastics. Polymer Engineering Science 1978;18;62-72.

[5] Barenblatt GI, 1959. The formation of equilibrium cracks during brittle fracture. General ideas and hypothesis. Axially-symmetric cracks, Prikl. Matem. I mekham 23, 434-444.

[6] Barenblatt GI, 1962. Mathematical theory of equilibrium cracks in brittle fracture. In: Dryden, H.L., von Karman, T. (Eds.), Advances in Applied Mechanics, vol. VII. Academic Press, New York, pp. 55-125.

[7] Dugdale DS, 1960. Yeilding of steel sheets containing slits. Journal of the Mechanics and Physics of Solids 8, 100 -104.

[8] Yan Y, Shang F, 2009. Cohesive zone modeling of interfacial delamination in PZT thin films. International Journal of Solids and Structures 46, 2739-2749.

[9] Jayaraman K, Reifsnider KL and Swain RE, 1993. Elastic and thermal effects in the interphase: part II. Comments on modeling studies. Journal of Composites Technology & Research 15 (1), 14–22.

[10] Xu XP, Needleman A, 1994. Numerical simulations of fast crack-growth in brittle solids. Journal of the Mechanics and Physics of Solids 42, 1397–1434.

[11] Tvergaard V, 1990. Effect of fibre debonding in a whisker-reinforced metal. Material Science and Engineering A 125 (2), 203–213.

[12] Camacho GT and Ortiz M, 1996. Computational modeling of impact damage in brittle materials. International Journal of Solids and Structures 33, 2899–2938.

[13] Geubelle PH and Baylor J, 1998. Impact-induced delamination of laminated composites: a 2D simulation. Composites Part B Engineering 29 (5), 589–602.

[14] Sarkar R, Banerjee R, Karami G and Azarmi F, 2010. Micromechanical model for examination and characterization of interfacial response of fibrous composites. ASME International Mechanical Engineering Congress and Exposition 2010-39984.

[15] Chandra N, Li H, Shet C and Ghonem H, 2002. Some issues in the application of cohesive zone models for metal–ceramic interfaces. International Journal of Solids and Structures 39, 2827-2855.

[16] Rao GVG, Mahajan P, Bhatnagar N. Micro-mechanical modeling of machining of FRP composites – Cutting force analysis. Composites Science Technology 2007;67;579-93.

[17] Dandekar CR, Shin YC. Multiphase Finite Element Modeling of Machining Unidirectional Composites: Prediction of Debonding and Fiber Damage. Journal of Manufacturing Science Engineering 2008;130;015016.1-015016.12.

[18] Fuchs PF, Major Z. Experimental determination of cohesive zone models for epoxy composites. Experimental Mechanics 2010;50;doi: 10.1007/s11340-010-9370-2.

[19] Alfano G, Crisfield MA. Finite element interface model for the delamination analysis of laminated composites: mechanical and computational issues. International Journal of Numerical Methods in Engineering 2001;50;1701-36.

[20] Ansys Inc. Theory Reference for the Mechanical APDL and Mechanical Applications. Release 12;Canonsburg, USA: SAS IP Inc.;2009

[21] Naik A, Abolfathi N, Karami G, Ziejewski M. Micromechanical viscoelastic characterization of fibrous composites. Journal of Composite Materials 2008;42;1179–1204.

[22] Hampe A, Marotzkea C. Experimental results of a pull-out test performed with single- and multi-fiber samples. Journal of Adhesion 2002;78;167-87.

[23] Zhandarov S, Pisanova E, Mäder E, Nairn JA. Investigation of load transfer between the fiber and the matrix in pull-out tests with fibers having different diameters. Journal of Adhesion Science Technology 2001;15;205-222.

[24] DiFrancia C, Ward TC, Claus RO. The single-fibre pull-out test. 1: Review and interpretation. Composites Part A 1996;27;597-612.

[25] Tsai K-H, Kim K-S. The micromechanics of fiber pull-out. Journal of the Mechanics and Physics of Solids 1996;44;1147-1177.

[26] Wool RP. The importance of interfaces in thermoplastic matrix composites and their tailoring during manufacture. Proceedings of the 28th Risø International Symposium on Materials Science. Interface Design of Polymer Matrix Composites – Mechanics, Chemistry, Modeling and Manufacturing.

[27] Baillie C, Emanuelsson J, Marton F. Building knowledge about the interface. Composites Part A 2001;32;305-312.

[28] Tenhaeff WE, Herbert EG, Pharr GM, Kalnaus S, Newman S, Sabau AS, Daniel C, Yu X, Hong K, Dudney NJ. Understanding the importance of interfaces in composites of solid polymer and glass electrolytes through modeling and electrochemical and mechanical characterizations. Symposium on energy storage beyond lithium ion: Materials Perspectives;2010.

[29] Fraunhofer Institute for Manufacturing Technology and Advanced Materials IFAM – Adhesive Bonding Technology and Surfaces. Fiber Composites - from matrix resins to the assembly of large structures. www.ifam.fraunhofer.de

[30] Multiscale Nanoscale Interface Engineering for Cement Composites. Multiscale Computational Mechanics Laboratory; Vanderbilt University School of Engineering.

[31] Foulk AJ, Fuqua MA, Ulven CA, Alcock MM. Flax fibre quality and influence on interfacial properties of composites. International Journal of Sustainable Engineering 2009;3:1;17-24.

[32] Yue CY, Padmanabhan K. Interfacial studies on surface modified Kevlar fiber/epoxy matrix composites. Composites: Part B 1999;30;205-217.

APPENDIX. AREA UNDER THE FORCE-DISPLACEMENT CURVE

```
clear all
clc
load my_xy.txt;
x=my_xy(:,1);
y=my_xy(:,2);
sum=0;
for i=1:362
   A(i,1)=x(i);
   A(i,2)=y(i);
end
a=0; b=0; c=0; d=0; F=0; G=0; Area=0;
for j=1:361
   a=A(j,1);
   b=A(j+1,1);
   c=A(j,2);
   d=A(j+1,2);
   F=c+d;
   G=b-a;
   Area=0.5*F*G;
   sum=sum+Area;
end
disp(sum);
```